

Enabling Massive Index Modulation Systems via Combinatorics-Free Detection

Hyeon Seok Rou, *Member, IEEE*, Giuseppe Thadeu Freitas de Abreu, *Senior Member, IEEE*, Takumi Takahashi, *Member, IEEE*, David González G., *Senior Member, IEEE*, and Osvaldo Gonsa.

Abstract—Index modulation (IM) is one of the key enabling technologies for beyond fifth generation (B5G) and sixth generation (6G) wireless systems, attracting attention for its inherent energy and spectral efficiency resulting from conveying information through the indexation of the resources utilized in during signal transmission. However, a remaining critical bottleneck for large-scale IM is the consequently infeasible detection complexity of combinatoric order. Therefore in this article, in order to maximally reap the advantages of IM in large scenarios, we propose a novel message passing (MP) decoder designed under the Gaussian belief propagation (GaBP) framework exploiting a novel unit vector decomposition (UVD) of IM signals with purpose-derived novel probability distributions. The proposed method enjoys a low decoding complexity that is independent of previously prohibitive combinatorial factors, while still approaching the performance of unfeasible state-of-the-art (SotA) search-based methods. The effectiveness of the proposed approach is demonstrated via complexity analysis and numerical results for the exemplary piloted generalized quadrature spatial modulation (GQSM) systems of truly massive sizes (up to 96 antennas).

Index Terms—Index modulation, quadrature spatial modulation, massive scale, message passing, low-complexity decoder.

I. INTRODUCTION

The expectations of beyond fifth generation (B5G) and sixth generation (6G) wireless systems prospect significant improvements over the existing systems in various different aspects including reliability, latency, energy and spectral efficiencies, coverage, user capacity, and more [2]–[5], motivating the investigation of a plethora of novel technologies such as millimeter-wave (mmWave)/Terahertz (THz) communications [6], [7], massive multiple-input multiple-output (mMIMO) and cell-free MIMO (CF-MIMO) [8], [9], reconfigurable intelligent surfaces (RISs) [10], [11], and integrated sensing and communications (ISAC) [12]–[15].

Among these many novel technologies, index modulation (IM) [16]–[20] has recently gained great attention as a potential enabling technology in its inherently high throughput, energy and spectral efficiencies. Specifically, this attractive and unique feature of enabling frugal utilization of resources at the transmitter is enabled by the activation of only small subsets of the totally available resources to encode information. This characteristic also lends IM schemes great flexibility, making it transparent to other promising technologies, as demonstrated by a quickly expanding literature on the integration of IM with classic communications concepts such as orthogonal frequency

division multiplex (OFDM) [21]–[24], multiple-input multiple-output (MIMO) [25]–[28], and multiple access [29], [30], and next-generation technologies such as RIS and ISAC [31]–[34].

Generally, an IM scheme activating P out of a total of N resources can convey up to $\lfloor \log_2 \binom{N}{P} \rfloor$ additional information bits on top of those conveyed over the selected P resources themselves, for example, via digital symbol modulation. Therefore, even with sufficiently large N and an adequate P , significant amounts of information can be encoded in the index domain, such to highlight the potential of IM to outperform conventional systems in certain scenarios [21], [35], with the added bonus of improving the energy-efficiency and freeing the unused resources to other functionalities, such as opportunistic communications and sensing [36], [37], etc.

The price of the aforementioned advantages of IM are, however, the burden cast onto the receiver in terms of the computational complexity required to detect the activated resources at each given transmission instance, given all possible resource activation patterns in the codebook of size $2^{\lfloor \log_2 \binom{N}{P} \rfloor}$. This challenge has therefore motivated work on low-complexity decoders for IM, in its many variations. To cite some examples, improvements over the brute-force maximum-likelihood (ML) search based on reduced-search methods such as lattice and sphere decoders [38], have decreased the total decoding complexity in proportion to the total codebook size, also by exploiting the specific IM design properties [22], [23], [39]. However, such methods are still generally dependent on the combinatorial factor, prohibitive for truly massive scales.

More recently, methods aiming to directly reduce the order of the binomial coefficient have also been proposed. In [40], for instance, the complexity order is reduced from $\binom{N}{P}$ to $\binom{\alpha N}{P}$ with $\frac{P}{N} \leq \alpha \leq 1$, by leveraging the orthogonal matching pursuit (OMP) algorithm to operate over the probable non-zero indices of the sparse signal of the generalized quadrature spatial modulation (GQSM), which is a specific type of IM. It was shown thereby that a trade-off between computational complexity and optimal performance can be achieved by adjusting the value of α . On the other hand, in [41], a GQSM detector leveraging the message passing (MP) algorithm with vector-valued variables under the Gaussian belief propagation (GaBP) framework is proposed, which reduces decoding cost to the order of the square root of the binomial coefficient, *i.e.*, $\binom{N}{P}^{\frac{1}{2}}$, while approaching the performance of ML solution. Finally, there exists also non-classical approaches which are independent of the binomial coefficient, including techniques based on machine learning (ML) [42], [43] and quantum computing (QC) [44]. Such alternatives have, nevertheless, their own limitations, such as the need for exhaustive off-line training or expensive and uncommon quantum computers.

H. S. Rou and G. T. F. de Abreu are with the School of Computer Science and Engineering, Constructor University, Campus Ring 1, 28759, Bremen, Germany (e-mails: [hrou, gabreu]@constructor.university).

T. Takahashi is with the Graduate School of Engineering, Osaka University, Suita 565-0871, Japan (e-mail: takahashi@comm.eng.osaka-u.ac.jp).

D. González G. and O. Gonsa are with Continental Automotive Technologies GmbH, Guerickestrasse 7, 60488, Frankfurt am Main, Germany (e-mails: david.gonzalez.g@ieee.org, osvaldo.gonsa@continental-corporation.com).

A part of this article has been presented at the *IEEE International Workshop on Computational Advances in Multi-Sensor Adaptive Processing, 2023* [1].

In light of all the above, we propose in this article a novel framework for IM detection which can enable a significantly reduced detection complexity that is complete independent of the prohibitive combinatorial factor inherent to IM, while still incorporating the elaborate combinatorial index codebook correlations. This is enabled by a novel unit vector decomposition (UVD) representation of IM signals, which reduce the effective signal space from the total signal vector variable into smaller unit vectors and scalars with significantly smaller effective signal spaces. Then, further aided by a novel statistical analysis of the non-trivial index-wide activation probabilities of the decoupled variables, tailored GaBP-based MP algorithms are designed to enable the concurrent estimation of the index activation information. On top of the achieved feasible complexity, the latter novel property also motivates massive IM schemes as a promising enabler of interference-free ISAC, by conducting information encoding only in the index domain whereas the resource-occupying signals can be utilized for sensing.

The effectiveness of the proposed framework is validated by simulations under the piloted GQSM variant of IM, which shows a reduced complexity where the full simulation results of unprecedented massive MIMO IM sizes (upto 96×96) was feasibly obtained with even a personal computer. In addition, several modifications to the transmitter pilot constellation design and the detection algorithm are also provided, which further enhance the performance of the proposed detector.

In all, our contributions can be summarized as follows:

- A novel detector for piloted IM schemes is designed under the GaBP framework, which enjoys a decoding complexity free of the combinatorics-dependent order.
- In order to enable the proposed detector, a novel UVD formulation of IM schemes and tailored MP rules are presented, with the derivation of closed-form index activation probability mass functions (PMFs) shown to match the empirical distributions exactly.
- Two enhancement modules for the proposed detector are presented, respectively based on successive interference cancellation (IC) and a conditional probability-based denoiser, in addition to a new mechanism to optimize the symbol constellation for the GQSM transmitter in order to improve its UVD-based detection performance.
- Simulation results and numerical and complexity analyses of the proposed detectors of truly massive GQSM systems are provided and compared against the state-of-the-art (SotA) detectors and fully multiplexed MIMO, with sizes upto 96×96 MIMO, which is unprecedented in related literature due to the infeasible detection complexity.

Notation: Complex scalars, vectors, and matrices are denoted by lowercase, boldface lowercase, and boldface uppercase characters, respectively, i.e., $x, \mathbf{x}, \mathbf{X}$. $\Re\{\cdot\}$ and $\Im\{\cdot\}$ denote the real and imaginary parts of a complex variable, while the superscripts $(\cdot)^R$ and $(\cdot)^I$ respectively denote variables which are *related* to the real and imaginary parts of the system, which may still be complex-valued. Other specific notations and functions are further defined in the text as necessary.

II. SYSTEM MODEL

As mentioned above, many SotA IM techniques can be found in the literature [16]–[47], [49]–[54] which address various issues of the problem such as integration with other functionalities (*e.g.* radar and/or sensing), achievable rates, decoding complexity and, of course which resource domains to exploit and under which architecture. Without loss of generality, we exemplify the derivation and analysis of the system and signal models with the GQSM [28], [40] design¹.

A. GQSM System Model and Transmitter Structure

Consider a point-to-point² (P2P) MIMO wireless communications system where the transmitter and the receiver are equipped with $N_T, N_R > 1 \in \mathbb{R}$ antennas, respectively, such that the receive signal $\mathbf{y} \in \mathbb{C}^{N_R \times 1}$ corresponding to the transmission of the information vector $\mathbf{x} \in \mathbb{C}^{N_T \times 1}$ through the flat-fading MIMO channel $\mathbf{H} \in \mathbb{C}^{N_R \times N_T}$ is described by

$$\mathbf{y} = \mathbf{H}\mathbf{x} + \mathbf{w} \in \mathbb{C}^{N_R \times 1}, \quad (1)$$

where $\mathbf{w} \in \mathbb{C}^{N_R \times 1}$ is a complex-valued additive white Gaussian noise (AWGN) vector with element-wise variance N_0 , such that $w_n \sim \mathcal{CN}(0, N_0)$.

In a GQSM transmitter, the in-phase and quadrature (IQ) components of P transmit symbols $\mathbf{s} = \{s_1^c, \dots, s_P^c\}$, taken from a complex-valued constellation \mathcal{S}^c of size $M \triangleq |\mathcal{S}^c|$, are sparsely mapped into the respective transmit vector components $\mathbf{x}^R \in \mathbb{C}^{N_T \times 1}$ and $\mathbf{x}^I \in \mathbb{C}^{N_T \times 1}$ of the form

$$\begin{aligned} \mathbf{x}^R &= [0, \dots, 0, \overbrace{s_1^R}^{k_1^R\text{-th position}}, 0, \dots, 0, \overbrace{s_p^R}^{k_p^R\text{-th position}}, 0, \dots, 0, \overbrace{s_P^R}^{k_P^R\text{-th position}}, 0]^T, \quad (2a) \\ \mathbf{x}^I &= [0, \overbrace{s_1^I}^{k_1^I\text{-th position}}, 0, \dots, 0, \overbrace{s_p^I}^{k_p^I\text{-th position}}, 0, \dots, 0, \overbrace{s_P^I}^{k_P^I\text{-th position}}, 0, \dots, 0]^T, \quad (2b) \end{aligned}$$

yielding the transmit signal vector

$$\mathbf{x} = \mathbf{x}^R + j\mathbf{x}^I \in \mathbb{C}^{N_T \times 1}. \quad (2c)$$

The positions of the IQ vector components in equation (2) are described by two independent index vectors $\mathbf{k}^R \triangleq [k_1^R, \dots, k_p^R, \dots, k_P^R]^T$ and $\mathbf{k}^I \triangleq [k_1^I, \dots, k_p^I, \dots, k_P^I]^T$ from the set of possible index vectors \mathcal{K} of size $Q \triangleq |\mathcal{K}|$. Specifically, $Q \triangleq 2^{\lfloor \log_2 \binom{N_T}{P} \rfloor}$, which implies that only binary-encodable subsets of the $\binom{N_T}{P}$ possible activation pattern combinations are utilized, such that the size of the GQSM IQ *activation vectors* codebook \mathcal{A} , is given by $|\mathcal{A}| = Q$.

Codebook Example: For the sake of clarity, consider a small system with $N_T = 5, P = 3$ with $\binom{5}{3} = 10$ activation vectors:

$$\left\{ \begin{bmatrix} s_1^x \\ s_2^x \\ s_3^x \\ 0 \\ 0 \end{bmatrix}, \begin{bmatrix} s_1^x \\ s_2^x \\ 0 \\ s_3^x \\ 0 \end{bmatrix}, \begin{bmatrix} s_1^x \\ s_2^x \\ 0 \\ 0 \\ s_3^x \end{bmatrix}, \begin{bmatrix} s_1^x \\ 0 \\ s_2^x \\ s_3^x \\ 0 \end{bmatrix}, \begin{bmatrix} s_1^x \\ 0 \\ s_2^x \\ 0 \\ s_3^x \end{bmatrix}, \begin{bmatrix} s_1^x \\ 0 \\ 0 \\ s_2^x \\ s_3^x \end{bmatrix}, \begin{bmatrix} 0 \\ s_1^x \\ s_2^x \\ s_3^x \\ 0 \end{bmatrix}, \begin{bmatrix} 0 \\ s_1^x \\ s_2^x \\ 0 \\ s_3^x \end{bmatrix}, \begin{bmatrix} 0 \\ s_1^x \\ 0 \\ s_2^x \\ s_3^x \end{bmatrix}, \begin{bmatrix} 0 \\ 0 \\ s_1^x \\ s_2^x \\ s_3^x \end{bmatrix} \right\},$$

where the non-zero elements s_p^x denote either s_p^R or s_p^I , since the signal codebooks for both IQ parts are identical.

¹It will be shown in Section III-B that the proposed design is applicable to any other type of IM-based scheme, by leveraging a UVD reformulation.

²The extension of the system model and the proposed techniques to a multi-user scenario requires addressing additional non-trivial challenges, most crucially the design of multi-user IM activation codebooks and the corresponding multi-user interference-aware detector designs, and therefore will be considered in a future work.

A valid codebook for such a system is a subset \mathcal{A} of the above, containing $Q \triangleq 2^{\lceil \log_2 \binom{5}{3} \rceil} = 8$ activation vectors, *e.g.*,

$$\mathcal{A} \triangleq \{\mathbf{a}_q\}_{q=1}^{Q=8} = \left\{ \begin{bmatrix} s_1^x \\ s_2^x \\ s_3^x \\ 0 \\ 0 \end{bmatrix}, \begin{bmatrix} s_1^x \\ s_2^x \\ 0 \\ 0 \\ s_3^x \end{bmatrix}, \begin{bmatrix} s_1^x \\ 0 \\ s_2^x \\ s_3^x \\ 0 \end{bmatrix}, \begin{bmatrix} s_1^x \\ 0 \\ s_2^x \\ 0 \\ s_3^x \end{bmatrix}, \begin{bmatrix} s_1^x \\ 0 \\ 0 \\ s_2^x \\ s_3^x \end{bmatrix}, \begin{bmatrix} 0 \\ s_1^x \\ s_2^x \\ s_3^x \\ 0 \end{bmatrix}, \begin{bmatrix} 0 \\ s_1^x \\ s_2^x \\ 0 \\ s_3^x \end{bmatrix}, \begin{bmatrix} 0 \\ s_1^x \\ 0 \\ s_2^x \\ s_3^x \end{bmatrix} \right\}, \quad (3)$$

which can be also represented by a corresponding set of *index vectors*, each of which contains the indices of the non-zero elements in the corresponding activation vector \mathbf{a}_q , that is

$$\mathcal{K} \triangleq \{\mathbf{k}_q\}_{q=1}^{Q=8} = \left\{ \begin{bmatrix} 1 \\ 2 \\ 3 \end{bmatrix}, \begin{bmatrix} 1 \\ 2 \\ 5 \end{bmatrix}, \begin{bmatrix} 1 \\ 3 \\ 4 \end{bmatrix}, \begin{bmatrix} 1 \\ 3 \\ 5 \end{bmatrix}, \begin{bmatrix} 1 \\ 4 \\ 5 \end{bmatrix}, \begin{bmatrix} 2 \\ 3 \\ 4 \end{bmatrix}, \begin{bmatrix} 2 \\ 3 \\ 5 \end{bmatrix}, \begin{bmatrix} 3 \\ 4 \\ 5 \end{bmatrix} \right\}. \quad (4)$$

It can be understood that obtaining a given codebook \mathcal{A} out of the larger set of $\binom{N_T}{P}$ possible activation vectors is a subject of optimization, and has been addressed, for instance, under a channel diversity criterion in [28], and under a decoding complexity criterion via QC in [47].

B. Reformulated System Model

In view of the formulation of GQSM transmit signals described in equation (2), the received signal model in equation (1) can be rewritten in the IQ-decoupled form as

$$\begin{bmatrix} \Re\{\mathbf{y}\} \\ \Im\{\mathbf{y}\} \end{bmatrix} = \underbrace{\begin{bmatrix} \Re\{\mathbf{H}\} & -\Im\{\mathbf{H}\} \\ \Im\{\mathbf{H}\} & \Re\{\mathbf{H}\} \end{bmatrix}}_{\triangleq \mathbf{H}} \underbrace{\begin{bmatrix} \mathbf{x}^R \\ \mathbf{x}^I \end{bmatrix}}_{\triangleq \mathbf{x}} + \underbrace{\begin{bmatrix} \Re\{\mathbf{w}\} \\ \Im\{\mathbf{w}\} \end{bmatrix}}_{\triangleq \mathbf{w}}, \quad (5)$$

where $\mathbf{y} \in \mathbb{R}^{2N_R \times 1}$, $\mathbf{x} \in \mathbb{R}^{2N_T \times 1}$, and $\mathbf{w} \in \mathbb{R}^{2N_R \times 1}$ denote the IQ-decoupled counterparts of \mathbf{y} , \mathbf{x} , and \mathbf{w} , respectively, and the IQ-decoupled channel matrix $\mathbf{H} \in \mathbb{R}^{2N_R \times 2N_T}$ is further decomposed into two submatrices as

$$\mathbf{H} = \begin{bmatrix} \underbrace{\Re\{\mathbf{H}\}}_{\triangleq \mathbf{H}^R} & \underbrace{-\Im\{\mathbf{H}\}}_{\triangleq \mathbf{H}^I} \\ \underbrace{\Im\{\mathbf{H}\}}_{\triangleq \mathbf{H}^I} & \underbrace{\Re\{\mathbf{H}\}}_{\triangleq \mathbf{H}^R} \end{bmatrix} = [\mathbf{H}^R \ \mathbf{H}^I], \quad (6)$$

with $\mathbf{H}^R \in \mathbb{R}^{2N_R \times N_T}$ and $\mathbf{H}^I \in \mathbb{R}^{2N_R \times N_T}$ denoting the effective channel components for \mathbf{x}^R and \mathbf{x}^I , respectively.

The real domain IQ-decoupled form $\mathbf{y} = \mathbf{H}\mathbf{x} + \mathbf{w}$ presented as equation (5) is the basis of most quadrature spatial modulation (QSM)/GQSM detection algorithms, which generally seek to solve the recovery problem

$$\hat{\mathbf{x}}_{\text{ML}} = \underset{\mathbf{x} \in \mathcal{X}}{\operatorname{argmin}} \|\mathbf{y} - \mathbf{H}\mathbf{x}\|_2^2, \quad (7)$$

where \mathcal{X} is the discrete domain of the effective signal \mathbf{x} , of cardinality $R \triangleq |\mathcal{X}| = (2^{\lceil \log_2 \binom{N_T}{P} \rceil})^2 \cdot M^P$.

The problem described by equation (7) is NP-hard due to the discrete solution domain \mathcal{X} , which prevents classical convex optimization approaches [48], requiring instead a combinatorial search over a high-dimensional space for optimal solution. To circumvent this challenge, SotA low-complexity solutions have been proposed by leveraging various characteristics of the GQSM signal. For example, the inherent sparsity of \mathbf{x} can be exploited by compressive sensing (CS)-based methods [49], [50], and the discrete codebook structure can be utilized to design search-based methods such as sphere decoders and

pruned-search decoders [39], [51], [52]. Finally, a vector-valued MP method was recently proposed in [41], where the two variables \mathbf{x}^R and \mathbf{x}^I are concurrently estimated by leveraging the independent and identically distributed (i.i.d.) bivariate property of the decoupled vectors in equation (6). The bivariate vector-valued MP method of [41] was shown to reduce the search space from $R = (2^{\lceil \log_2 \binom{N_T}{P} \rceil})^2 \cdot M^P$ to $2\sqrt{R} = 2 \cdot (2^{\lceil \log_2 \binom{N_T}{P} \rceil}) \cdot (\sqrt{M})^P$.

Building on the above, we propose in the sequel a novel low-complexity decoder, which leverages a new UVD-based GQSM system model integrated into the GaBP framework with purpose-derived index activation probability distributions, to achieve a remarkably low decoding complexity order that is entirely independent of the combinatorial factor $\binom{N_T}{P}$.

III. PROPOSED UVD-BASED SYSTEM REFORMULATION

In this section, the proposed unit vector decomposition (UVD) of the GQSM system model and the derivation of the novel index activation probability distributions arising from this decomposition are presented. As shall be clarified, the resultant index-wise distributions enable the design of an MP algorithm operating on a combinatorics-free signal domain.

A. Unit Vector Decomposition (UVD) of GQSM Scheme

First, notice that each IQ symbol component s_p^R and s_p^I occupies a single position in the GQSM transmit vector \mathbf{x} described in equation (2), which can therefore be rewritten as a superposition of the symbol components multiplied by *elementary activation vectors* \mathbf{e}_t , yielding

$$\mathbf{x} = \underbrace{\left(\sum_{p=1}^P s_p^R \mathbf{e}_{k_p^R} \right)}_{\triangleq \mathbf{x}^R} + j \underbrace{\left(\sum_{p=1}^P s_p^I \mathbf{e}_{k_p^I} \right)}_{\triangleq \mathbf{x}^I} \in \mathbb{C}^{N_T \times 1}, \quad (8)$$

where $\mathbf{e}_t \in \{0, 1\}^{N_T}$, with $t \in \mathcal{T} \triangleq \{1, \dots, N_T\}$, is the t -th column of an $N_T \times N_T$ identity matrix \mathbf{I}_{N_T} , which defines the set \mathcal{E} of orthonormal unit vectors on $\{0, 1\}^{N_T}$ as

$$\mathcal{E} \triangleq \{\mathbf{e}_t\}_{t=1}^{N_T} = \left\{ \begin{bmatrix} 1 \\ 0 \\ \vdots \\ 0 \end{bmatrix}, \begin{bmatrix} 0 \\ 1 \\ \vdots \\ 0 \end{bmatrix}, \dots, \begin{bmatrix} 0 \\ 0 \\ \vdots \\ 1 \end{bmatrix} \right\}. \quad (9)$$

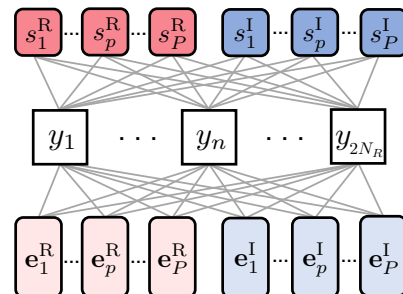


Fig. 1: Multivariate bilinear factor graph with $2P$ symbol variables and $2P$ unit vector variables, as per equation (10).

Then, by reformulating the transmit vector \mathbf{x} , the IQ-decoupled received signal vector of equation (5) becomes

$$\mathbf{y} = \mathbf{H} \left[\sum_{p=1}^P s_p^R \mathbf{e}_{k_p^R} \right] + \mathbf{w} \in \mathbb{R}^{2N_R \times 1}, \quad (10)$$

which better highlights the construct of the GQSM signals with inherently independent spatial and digital encoding, as illustrated by the bilinear factor graph shown in Fig. 1.

In other words, the estimation of the full effective signal \mathbf{x} has been transformed into the joint estimation problem of $2P$ activation vectors and P transmit symbols, which also enables independent estimation techniques when some of the decoupled variables are known, *i.e.*, via pilot symbols.

B. UVD Model for Coded and Space-time Coded IM

The UVD model described above works for all spatial modulation (SM) schemes whose activation vectors are directly given by the unit vectors in \mathcal{E} , *e.g.*, generalized spatial modulation (GSM) and GQSM. There exists, however, enhanced SM-based schemes [53], [54] whose transmit symbols are not multiplied by elementary activation vectors in the space of $\{0, 1\}^{N_T}$, but by optimized precoded *dispersion vectors* drawn from a complex space \mathbb{C}^{N_T} .

Let then $\mathcal{D}^R \triangleq \{\mathbf{d}_q^R\}_{q=1}^Q \in \mathbb{C}^{N_T \times 1}$ and $\mathcal{D}^I \triangleq \{\mathbf{d}_q^I\}_{q=1}^Q \in \mathbb{C}^{N_T \times 1}$ be the sets from which the precoded dispersion vectors of a generic coded SM are drawn. Then, the corresponding transmit signal vector is given by

$$\mathbf{x} = \left(\sum_{p=1}^P s_p^R \mathbf{d}_{k_p^R}^R \right) + j \left(\sum_{p=1}^P s_p^I \mathbf{d}_{k_p^I}^I \right) \in \mathbb{C}^{N_T \times 1}. \quad (11)$$

Next, we leverage the trivial identities

$$\mathbf{d}_q^R \triangleq \overbrace{[\mathbf{d}_1^R, \dots, \mathbf{d}_Q^R]}^{\triangleq \mathbf{\Xi}^R \in \mathbb{C}^{N_T \times Q}} \cdot \mathbf{e}_q \quad \text{and} \quad \mathbf{d}_q^I \triangleq \overbrace{[\mathbf{d}_1^I, \dots, \mathbf{d}_Q^I]}^{\triangleq \mathbf{\Xi}^I \in \mathbb{C}^{N_T \times Q}} \cdot \mathbf{e}_q, \quad (12)$$

with $\mathbf{e}_q \in \{0, 1\}^{Q \times 1}$, to rewrite equation (11) as

$$\mathbf{x} = \mathbf{\Xi}^R \left(\sum_{p=1}^P s_p^R \mathbf{e}_{k_p^R} \right) + j \mathbf{\Xi}^I \left(\sum_{p=1}^P s_p^I \mathbf{e}_{k_p^I} \right) \in \mathbb{C}^{N_T \times 1}, \quad (13)$$

where $\mathbf{\Xi}^R \in \mathbb{C}^{N_T \times Q}$ and $\mathbf{\Xi}^I \in \mathbb{C}^{N_T \times Q}$ are the dispersion vector codebook matrices constructed by concatenating the Q dispersion vectors in \mathcal{D}^R and \mathcal{D}^I respectively³

Then, the IQ-decoupled form of the received signal corresponding to the transmit vector in equation (13) becomes

$$\begin{aligned} \mathbf{y} &= \mathbf{H} \overbrace{\left[\begin{array}{c} \Re\{\mathbf{\Xi}^R\} - \Im\{\mathbf{\Xi}^I\} \\ \Im\{\mathbf{\Xi}^R\} \quad \Re\{\mathbf{\Xi}^I\} \end{array} \right]}^{\triangleq \mathbf{\Xi} \in \mathbb{R}^{2N_T \times 2Q}} \left[\begin{array}{c} \sum_{p=1}^P s_p^R \mathbf{e}_{k_p^R} \\ \sum_{p=1}^P s_p^I \mathbf{e}_{k_p^I} \end{array} \right] + \mathbf{w}, \\ &= \tilde{\mathbf{H}} \left[\begin{array}{c} \sum_{p=1}^P s_p^R \mathbf{e}_{k_p^R} \\ \sum_{p=1}^P s_p^I \mathbf{e}_{k_p^I} \end{array} \right] + \mathbf{w} \in \mathbb{R}^{2N_R \times 1}, \end{aligned} \quad (14)$$

where the effective channel $\tilde{\mathbf{H}} \triangleq \mathbf{H}\mathbf{\Xi} \in \mathbb{R}^{2N_R \times 2Q}$ is constructed from the dispersion codebook $\mathbf{\Xi}$ and the channel state information (CSI) \mathbf{H} , both known at the receiver.

³ It can be seen that the formulation for the GQSM system described by equations (8) and (10) is the simplified case of this generalized UVD form, as the matrices $\mathbf{\Xi}^R$ and $\mathbf{\Xi}^I$ reduce to the identity matrix in the GQSM case.

The structural equivalence between equations (14) and (10) is clear, from which it is evident that the decoding method to be described in Section IV can be applied to both cases. Following similar steps, it can be also shown that IM schemes incorporating space-time coding (STC), such as those proposed in [28], [39], in which dispersion vectors are generalized into dispersion matrices of size $N_T \times T$ with T consecutive symbol periods, can also be represented, via a vectorization of the system model, by the same UVD formulation shown above, once again enabling the proposed technique of Section IV to be applied.

To elaborate, given the sets of dispersion *matrices* $\mathcal{D}^R \triangleq \{\mathbf{D}_q^R\}_{q=1}^Q \in \mathbb{C}^{N_T \times T}$ and $\mathcal{D}^I \triangleq \{\mathbf{D}_q^I\}_{q=1}^Q \in \mathbb{C}^{N_T \times T}$, the transmit signal of a STC-based IM scheme becomes

$$\mathbf{X} = \left(\sum_{p=1}^P s_p^R \mathbf{D}_{k_p^R}^R \right) + j \left(\sum_{p=1}^P s_p^I \mathbf{D}_{k_p^I}^I \right) \in \mathbb{C}^{N_T \times T}, \quad (15)$$

whose vectorized form is trivially given as

$$\text{vec}(\mathbf{X}) = \left(\sum_{p=1}^P s_p^R \text{vec}(\mathbf{D}_{k_p^R}^R) \right) + j \left(\sum_{p=1}^P s_p^I \text{vec}(\mathbf{D}_{k_p^I}^I) \right) \in \mathbb{C}^{TN_T \times 1}. \quad (16)$$

The UVD representation of equation (16) is therefore similar to that of equation (13), except for the increased dimensionality to TN_T , and the dictionary matrices of vectorized dispersion matrices $\mathbf{\Xi}^R \triangleq [\text{vec}(\mathbf{D}_1^R), \dots, \text{vec}(\mathbf{D}_Q^R)] \in \mathbb{C}^{TN_T \times Q}$ and $\mathbf{\Xi}^I \triangleq [\text{vec}(\mathbf{D}_1^I), \dots, \text{vec}(\mathbf{D}_Q^I)] \in \mathbb{C}^{TN_T \times Q}$, which yields the vectorized received signal model

$$\begin{aligned} \mathbf{y} &\triangleq \text{vec}(\mathbf{Y}) = \text{vec}(\mathbf{H}\mathbf{X} + \mathbf{W}), \\ &= (\mathbf{I}_T \otimes \mathbf{H}) \left[\begin{array}{c} \Re\{\mathbf{\Xi}^R\} - \Im\{\mathbf{\Xi}^I\} \\ \Im\{\mathbf{\Xi}^R\} \quad \Re\{\mathbf{\Xi}^I\} \end{array} \right] \left[\begin{array}{c} \sum_{p=1}^P s_p^R \mathbf{e}_{k_p^R} \\ \sum_{p=1}^P s_p^I \mathbf{e}_{k_p^I} \end{array} \right] + \text{vec}(\mathbf{W}), \\ &= \tilde{\mathbf{H}} \left[\begin{array}{c} \sum_{p=1}^P s_p^R \mathbf{e}_{k_p^R} \\ \sum_{p=1}^P s_p^I \mathbf{e}_{k_p^I} \end{array} \right] + \tilde{\mathbf{w}} \in \mathbb{R}^{2TN_R \times 1}, \end{aligned} \quad (17)$$

where \mathbf{I}_T is the $T \times T$ identity matrix, the symbol \otimes denotes Kronecker product, and $\tilde{\mathbf{H}}$ and $\tilde{\mathbf{w}}$ are the augmented effective channel matrix and AWGN vector, respectively.

From the equivalence among equations (17), (14) and (10), it follows once again that the UVD model introduced in (III-A) for the GQSM scheme generalizes to other IM methods in other domains and higher dimensions. Therefore, we emphasize again that all of the following derivations, analyses, and proposed methods are applicable to all general types of IM. However, for the sake of simplicity, the remainder of the article will continue to use the GQSM scheme as an exemplary case.

C. Prior Distribution of Unit Vector Variables

Let us now proceed to analyze the prior distributions of the two sets of variables in the UVD model, namely the IQ symbol components s_p^R and s_p^I , and the elementary activation vectors $\mathbf{e}_{k_p^R}$ and $\mathbf{e}_{k_p^I}$, respectively, in order to enable their estimation via Bayesian inference methods.

Since QSM schemes typically employ complex symmetric constellations⁴ such as M -quadrature amplitude modulation (QAM), s_p^R and s_p^I and belong to the corresponding real-valued effective constellation $\mathcal{S} \triangleq \Re\{\mathcal{S}^c\} = \Im\{\mathcal{S}^c\}$, which is typically a pulse amplitude modulation (PAM) constellation of cardinality $|\mathcal{S}| \triangleq \sqrt{M}$.

Succinctly, we therefore have

$$s_p^R, s_p^I \sim \mathbb{P}_s(s_p) \triangleq \sum_{s \in \mathcal{S}} \frac{1}{\sqrt{M}} \cdot \delta(s - s_p). \quad (18)$$

On the other hand, the PMF of $e_{k_p^R}$ and $e_{k_p^I}$ is not so trivial, and is given by

$$\mathbf{e}_{k_p^R}, \mathbf{e}_{k_p^I} \sim \mathbb{P}_{\mathbf{e}_{k_p}}(\mathbf{e}_{k_p}) \triangleq \sum_{\mathbf{e}_t \in \mathcal{E}} \mathbb{P}_{\mathbf{e}_{k_p}}(\mathbf{e}_{k_p} = \mathbf{e}_t) \cdot \delta(\mathbf{e}_{k_p} - \mathbf{e}_t), \quad (19)$$

which can be alternatively described solely in terms of the corresponding activation indices k_p^R and k_p^I , such that equation (19) can equivalently be written as

$$k_p^R, k_p^I \sim \mathbb{P}_{k_p}(k_p) \triangleq \sum_{t \in \mathcal{T}} \mathbb{P}_{k_p}(k_p = t) \cdot \delta(k_p - t). \quad (20)$$

The challenge in equation (20) lies in the probabilities $\mathbb{P}_{k_p}(k_p)$, which far from being uniform and independent, is strongly correlated and differs significantly for each p , as a consequence of the combinatorial selection which yields finite and ordered index lists. To illustrate, consider the example shown in equation (4) for $N_T = 5$ and $P = 3$, from which it can be seen that the first element k_1 has a higher probability of taking on the value of 1, then 2 and 3, and can never take on the values 4 or 5. Similar restrictions apply for the other index vector elements k_2 and k_3 .

Fortunately, the analytical PMFs corresponding to the index vector elements $k_p, \forall p$, can be derived using tools of numerical and combinatorial analysis [55]–[57]. In particular, consider the following bounded variations of Bernstein polynomials [57] on the discrete variable $t \in \mathcal{T} \triangleq \{1, \dots, N_T\}$ given by

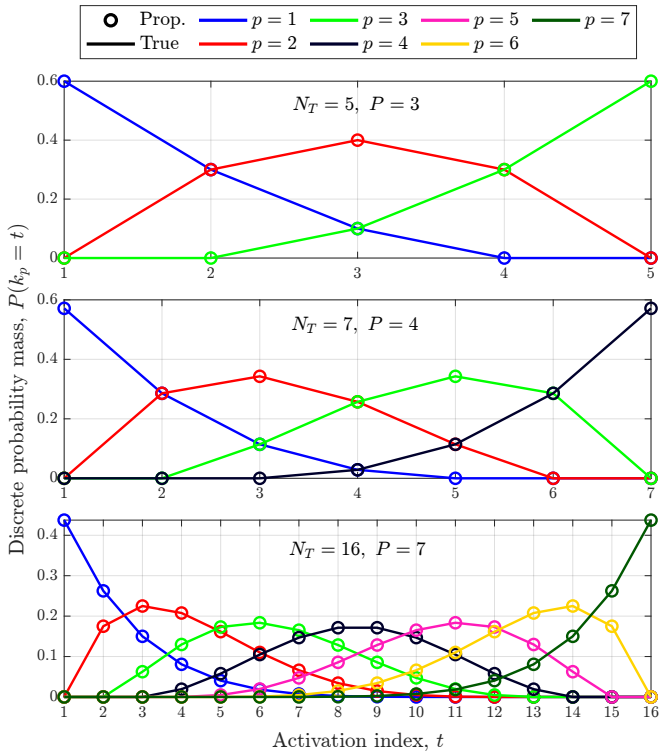


Fig. 2: Comparison of discrete polynomial-based PMF and empirically-obtained distribution of the activation indices of the index vectors in \mathcal{K} .

$$R_p^P(t; N_T) = \begin{cases} \frac{(t-1)(N_T-t)!}{(t-p)!((N_T-t)-(P-p))!} & \text{if } t \text{ satisfies eq. (22),} \\ 0 & \text{otherwise,} \end{cases} \quad (21)$$

where

$$(p-1) < t < (N_T - P - p + 1). \quad (22)$$

For each value p , the polynomial $R_p^P(t; N_T)$ gives the number of the mutually exclusive index t , out of a list of length P , confined to the interval \mathcal{T} , such that the desired distributions are obtained by merely normalizing such polynomials, yielding

$$\mathbb{P}_{k_p}(k_p = t) = \frac{R_p^P(t; N_T)}{\sum_{t \in \mathcal{T}} R_p^P(t; N_T)} \triangleq \mathbb{P}_{\mathbf{e}_{k_p}}(\mathbf{e}_{k_p} = \mathbf{e}_t). \quad (23)$$

Some examples of the PMF given by equation (23) are compared to the true empirical distributions in Figure 2, for various N_T and P , which confirm that the expression is exact.

For future convenience, the probability masses of the PMF $\mathbb{P}_{\mathbf{e}_{k_p}}(\mathbf{e}_{k_p})$ is represented by the vector \mathbf{r}_p defined as

$$\mathbf{r}_p \triangleq [\mathbb{P}_{\mathbf{e}_{k_p}}(\mathbf{e}_{k_p} \triangleq \mathbf{e}_1), \dots, \mathbb{P}_{\mathbf{e}_{k_p}}(\mathbf{e}_{k_p} = \mathbf{e}_{N_T})]^T \in \mathbb{R}^{N_T \times 1}. \quad (24)$$

IV. PROPOSED LOW-COMPLEXITY DETECTOR FOR PILOTTED MASSIVE INDEX MODULATION SCHEMES

With possession of the analytical prior PMFs of the indices k_p given in equations (18) and (23), respectively, we next design a GaBP-based MP algorithm for their estimation. In particular, we will derive the MP rules for a piloted GQSM, *i.e.*, where $s_p^R, s_p^I \forall p$ are known, which can be utilized to enable secondary functionalities⁵ such as sensing [58]–[61], as well as communication via the detection of activation patterns.

First, the soft-replicas for the activation vector variables $\mathbf{e}_{k_p^R}$ and $\mathbf{e}_{k_p^I}$ with $p \in \{1, \dots, P\}$ are defined for the n -th factor node (*i.e.*, n -th pilot) with $n \in \{1, \dots, 2N_R\}$, as $\hat{\mathbf{e}}_{k_p^R:n}$ and $\hat{\mathbf{e}}_{k_p^I:n}$, respectively, as illustrated in the factor graph of Figure 1. The corresponding error covariance matrices of the activation vector soft-replicas are defined as

$$\mathbf{\Gamma}_{p:n}^R \triangleq \mathbb{E}_{\mathbf{e}_{k_p}}[(\mathbf{e}_{k_p} - \hat{\mathbf{e}}_{k_p^R:n})(\mathbf{e}_{k_p} - \hat{\mathbf{e}}_{k_p^R:n})^H] \in \mathbb{R}^{N_T \times N_T}, \quad (25a)$$

$$= \sum_{\mathbf{e}_t \in \mathcal{E}} (\mathbb{P}_{\mathbf{e}_{k_p}}(\mathbf{e}_{k_p} = \mathbf{e}_t) \cdot (\mathbf{e}_t - \hat{\mathbf{e}}_{k_p^R:n})(\mathbf{e}_t - \hat{\mathbf{e}}_{k_p^R:n})^H),$$

$$\mathbf{\Gamma}_{p:n}^I \triangleq \mathbb{E}_{\mathbf{e}_{k_p}}[(\mathbf{e}_{k_p} - \hat{\mathbf{e}}_{k_p^I:n})(\mathbf{e}_{k_p} - \hat{\mathbf{e}}_{k_p^I:n})^H] \in \mathbb{R}^{N_T \times N_T}, \quad (25b)$$

$$= \sum_{\mathbf{e}_t \in \mathcal{E}} (\mathbb{P}_{\mathbf{e}_{k_p}}(\mathbf{e}_{k_p} = \mathbf{e}_t) \cdot (\mathbf{e}_t - \hat{\mathbf{e}}_{k_p^I:n})(\mathbf{e}_t - \hat{\mathbf{e}}_{k_p^I:n})^H),$$

where the expectation is taken over the corresponding unique PMFs of equation (23), for each $p \in \{1, \dots, P\}$.

Remark: It can be seen from equation (25) and the system analysis in Section II, that the derivations corresponding to the two IQ components are identical. Therefore, for the sake of brevity, we hereafter derive expressions only for the real components, with the understanding that the same results apply to the imaginary components, only with the terms $(\cdot)^R$ replaced by $(\cdot)^I$.

⁴If that is not the case, and \mathcal{S}^c is irregular, the formulation is trivially generalized by considering distinct PAM constellations for s_p^R and s_p^I .

⁵We highlight that, in principle, a bilinear MP decoder for this system could also be developed [61]–[64], such that some of the pilots could be replaced by information-carrying symbols to increase the rate of communications, albeit at the expense of some performance degradation. Such extension is out of scope of the current article and will be pursued in a follow-up work.

Computed naively, the covariances in equation (25) requires a summation of N_T outer products of dimensions $N_T \times N_T$, with complexity $\mathcal{O}(N_T^3)$. Thanks to the UVD and the sparsity of the unit vectors in \mathcal{E} , however, equation (25) can be put into the following closed-form of associated complexity $\mathcal{O}(N_T^2)$,

$$\mathbf{\Gamma}_{p:n}^R = \text{diag}(\mathbf{r}_p) + \hat{\mathbf{e}}_{k_p^R:n} \hat{\mathbf{e}}_{k_p^R:n}^T - (\mathbf{E}_{p:n}^R + (\mathbf{E}_{p:n}^R)^T), \quad (26)$$

where the $N_T \times N_T$ square matrix $\mathbf{E}_{p:n}^R$ is given by

$$\mathbf{E}_{p:n}^R \triangleq \mathbf{r}_p^T \otimes \hat{\mathbf{e}}_{k_p^R:n} = [r_{p(1)} \cdot \hat{\mathbf{e}}_{k_p^R:n}, \dots, r_{p(N_T)} \cdot \hat{\mathbf{e}}_{k_p^R:n}], \quad (27)$$

with $r_{p(t)}$ denoting the t -th element of the vector of probability mass coefficients of \mathbf{r}_p from equation (24).

In hand of the soft-replica vectors and the error covariance matrices, the $2N_R$ factor nodes corresponding to the received symbols in \mathbf{y} , each perform soft-IC on the received symbols y_n for the activation vectors as

$$\bar{y}_{p:n}^R = y_n - (\mathbf{h}_n^R)^T \sum_{p' \neq p} (s_{p'}^R \hat{\mathbf{e}}_{k_{p'}^R:n}) - (\mathbf{h}_n^I)^T \sum_{p'=1}^P (s_{p'}^I \hat{\mathbf{e}}_{k_{p'}^I:n}), \quad (28)$$

where $(\mathbf{h}_n^R)^T \in \mathbb{R}^{1 \times N_T}$ and $(\mathbf{h}_n^I)^T \in \mathbb{R}^{1 \times N_T}$ respectively denote the n -th rows of the channel components $\mathbf{H}^R \in \mathbb{R}^{2N_T \times N_T}$ and $\mathbf{H}^I \in \mathbb{R}^{2N_T \times N_T}$ which are defined in equation (6).

As can be seen in equation (29) at the bottom of the page, the soft-IC symbol is comprised of the true symbol part and a term related to the soft-replica error plus AWGN, such that the latter term can be approximated by a Gaussian scalar via the central limit theorem (CLT), which yields the conditional probability density functions (PDFs) of the soft-IC symbols conditional to a given activation vector as

$$\mathbb{P}(\bar{y}_{p:n}^R | \mathbf{e}_{k_p^R}) \propto \exp\left(-\frac{|\bar{y}_{p:n}^R - s_p^R (\mathbf{h}_n^R)^T \mathbf{e}_{k_p^R}|^2}{\nu_{p:n}^R}\right), \quad (30)$$

where the conditional variance $\nu_{p:n}^R$ is obtained via

$$\begin{aligned} \nu_{p:n}^R &= \mathbb{E}_{\mathbf{e}_{k_p^R}} \left[|\bar{y}_{p:n}^R - s_p^R (\mathbf{h}_n^R)^T \mathbf{e}_{k_p^R}|^2 \right] \\ &= \nu_n - (\mathbf{h}_n^R)^T (|s_p^R|^2 \cdot \mathbf{\Gamma}_{p:n}^R) (\mathbf{h}_n^R)^* + \frac{N_0}{2}, \end{aligned} \quad (31)$$

with the total variance ν_n prior to the soft-IC

$$\nu_n \triangleq (\mathbf{h}_n^R)^T \left(\sum_{p=1}^P |s_p^R|^2 \cdot \mathbf{\Gamma}_{p:n}^R \right) (\mathbf{h}_n^R)^* + (\mathbf{h}_n^I)^T \left(\sum_{p=1}^P |s_p^I|^2 \cdot \mathbf{\Gamma}_{p:n}^I \right) (\mathbf{h}_n^I)^* \quad (32)$$

The conditional PDFs of equation (30) are combined at the variable nodes to obtain the extrinsic belief $b_{p:n}^R$, *i.e.*,

$$\begin{aligned} \mathbb{P}(b_{p:n}^R | \mathbf{e}_{k_p^R}) &= \prod_{n' \neq n} \mathbb{P}(\bar{y}_{p:n'}^R | \mathbf{e}_{k_p^R}) \\ &\propto \exp\left((\boldsymbol{\eta}_{p:n}^R)^T \mathbf{e}_{k_p^R} - \frac{1}{2} (\mathbf{e}_{k_p^R})^T \boldsymbol{\Lambda}_{p:n}^R \mathbf{e}_{k_p^R}\right), \end{aligned} \quad (33)$$

where self-IC is included for the computation of the extrinsic belief for the n -th factor node, as can be seen by the exclusion of the n -th conditional PDF from the variable node.

The resulting unscaled multivariate Gaussian PDF of the extrinsic beliefs are efficiently described in terms of the information vector $\boldsymbol{\eta}_{p:n}^R \in \mathbb{R}^{N_T \times 1}$, which is given by

$$\boldsymbol{\eta}_{p:n}^R = s_p^R \sum_{n' \neq n} \frac{\bar{y}_{p:n'}^R}{\nu_{p:n'}^R} \mathbf{h}_{n'}^R, \quad (34)$$

and in terms of the precision matrix $\boldsymbol{\Lambda}_{p:n}^R \in \mathbb{R}^{N_T \times N_T}$ given by

$$\boldsymbol{\Lambda}_{p:n}^R = |s_p^R|^2 \sum_{n' \neq n} \frac{\mathbf{h}_{n'}^R (\mathbf{h}_{n'}^R)^T}{\nu_{p:n'}^R}. \quad (35)$$

In turn, the posterior Bayes-optimal soft-replicas are computed from the extrinsic beliefs via

$$\begin{aligned} \hat{\mathbf{e}}_{k_p^R:n} &= \frac{\mathbb{E}_{\mathbf{e}_{k_p^R}} [\mathbf{e}_{k_p^R} \cdot \mathbb{P}(b_{p:n}^R | \mathbf{e}_{k_p^R})]}{\mathbb{E}_{\mathbf{e}_{k_p^R}} [\mathbb{P}(b_{p:n}^R | \mathbf{e}_{k_p^R})]} \in \mathbb{R}^{N_T \times 1} \\ &= \frac{\sum_{\mathbf{e}_t \in \mathcal{E}} (\mathbf{e}_t \cdot \mathbb{P}_{\mathbf{e}_{k_p^R}}(\mathbf{e}_{k_p^R} = \mathbf{e}_t) \cdot \mathbb{P}(b_{p:n}^R | \mathbf{e}_{k_p^R}))}{\sum_{\mathbf{e}_t \in \mathcal{E}} (\mathbb{P}_{\mathbf{e}_{k_p^R}}(\mathbf{e}_{k_p^R} = \mathbf{e}_t) \cdot \mathbb{P}(b_{p:n}^R | \mathbf{e}_{k_p^R}))}, \end{aligned} \quad (36)$$

Similarly to equation (25), the expectation of $\mathbf{e}_{k_p^R}$ over its domain \mathcal{E} can be efficiently described in a closed-form expression with reduced computational complexity, namely

$$\hat{\mathbf{e}}_{k_p^R:n} = \frac{\mathbf{r}_p \odot \mathbf{z}_{p:n}^R}{\mathbf{r}_p^T \cdot \mathbf{z}_{p:n}^R} \in \mathbb{R}^{N_T \times 1}, \quad (37)$$

where the vector of unnormalized belief mass $\mathbf{z}_{p:n}^R$ is given by

$$\begin{aligned} \mathbf{z}_{p:n}^R &= \exp_{\odot}(\boldsymbol{\eta}_{p:n}^R - \frac{1}{2} \text{diag}(\boldsymbol{\Lambda}_{p:n}^R)) \in \mathbb{R}^{N_T \times 1}, \\ &= [e^{\boldsymbol{\eta}_{p:n}^R(1) - \frac{1}{2} \boldsymbol{\Lambda}_{p:n}^R(1,1)}, \dots, e^{\boldsymbol{\eta}_{p:n}^R(N_T) - \frac{1}{2} \boldsymbol{\Lambda}_{p:n}^R(N_T, N_T)}]^T, \end{aligned} \quad (38)$$

with $\exp_{\odot}(\cdot)$ denoting the element-wise exponentiation of a vector, $\boldsymbol{\eta}_{p:n}^R(t)$ denoting the elements at the t -th position of the vector $\boldsymbol{\eta}_{p:n}^R$, and $\boldsymbol{\Lambda}_{p:n}^R(t,t)$ denoting the elements at the (t,t) -th position of the matrix $\boldsymbol{\Lambda}_{p:n}^R$.

Notice that equation (38) clarifies that only the diagonal elements of the precision matrix are required for the computation of the soft-replica vectors. Therefore, instead of computing the entire precision matrix as in equation (35), the vector of diagonal elements can be directly obtained to significantly improve the computational complexity, given by

$$\text{diag}(\boldsymbol{\Lambda}_{p:n}^R) = |s_p^R|^2 \sum_{n' \neq n} \frac{|\mathbf{h}_{n'}^R|^2}{\nu_{p:n'}^R} \quad (39)$$

where $|\cdot|_{\odot}$ denotes the element-wise absolute value operator.

Equations (28) to (39) describe the steps of one MP iteration to estimate the $2P$ activation vectors of the piloted GQSM with UVD, which yields the refined posterior soft-replica vectors and the corresponding error covariance matrices.

At the end of a τ -th MP iteration, the soft-replica vectors and error covariance matrices are damped [65] in order to prevent early convergence to a local optima [66], thus

$$\hat{\mathbf{e}}_{k_p^R:n}^{[\tau+1]} \leftarrow \rho \cdot \hat{\mathbf{e}}_{k_p^R:n}^{[\tau]} + (1 - \rho) \cdot \hat{\mathbf{e}}_{k_p^R:n}^{[\tau+1]}, \quad (40)$$

where $\rho \in [0, 1]$ is the damping factor, and the superscript $(\cdot)^{[\tau]}$ denotes the τ -th iterate of the variable.

$$\bar{y}_{p:n}^R \triangleq \overbrace{(\mathbf{h}_n^R)^T s_p^R \hat{\mathbf{e}}_{k_p^R:n}}^{\text{True symbol}} + \overbrace{(\mathbf{h}_n^R)^T \sum_{p' \neq p} s_{p'}^R (\mathbf{e}_{k_{p'}^R} - \hat{\mathbf{e}}_{k_{p'}^R:n}) + (\mathbf{h}_n^I)^T \sum_{p'=1}^P s_{p'}^I (\mathbf{e}_{k_{p'}^I} - \hat{\mathbf{e}}_{k_{p'}^I:n}) + w_n}_{\text{Scalar Gaussian approximation (SGA)}}, \quad (29)$$

The last of the MP iterations, denoted by the index τ_{conv} , can be determined by well-known convergence criteria, such as the maximum number of iterations, *i.e.*, while $\tau \leq \tau_{\text{max}}$, or a given convergence threshold of the soft-replicas *i.e.*, while $|\hat{\mathbf{e}}_{k_p^R:n}^{[\tau+1]} - \hat{\mathbf{e}}_{k_p^R:n}^{[\tau]}| > \varepsilon_{\text{Th}}$. After the last MP iteration, a belief consensus is taken over the $2N_R$ factor nodes via

$$\mathbb{P}(b_p^R | \mathbf{e}_{k_p^R}) = \prod_{n=1}^{2N_R} \mathbb{P}(\bar{y}_{p:n}^R | \mathbf{e}_{k_p^R}) \propto \exp((\boldsymbol{\eta}_p^R)^\top \mathbf{e}_{k_p^R} - \frac{1}{2} (\mathbf{e}_{k_p^R})^\top \boldsymbol{\Lambda}_p^R \mathbf{e}_{k_p^R}), \quad (41)$$

which is equivalent to equation (33) without the self-interference cancellation operation.

Similarly, the consensus information vectors and precision matrix diagonals are respectively given by

$$\boldsymbol{\eta}_p^R = s_p^R \sum_{n=1}^{2N_R} \frac{\bar{y}_{p:n}^R}{\nu_{p:n}^R} \mathbf{h}_n^R, \quad (42)$$

$$\text{diag}(\boldsymbol{\Lambda}_p^R) = |s_p^R|^2 \sum_{n=1}^{2N_R} \frac{|\mathbf{h}_n^R|_{\odot}^2}{\nu_{p:n}^R}, \quad (43)$$

Finally, a hard-decision on the $2P$ activation vectors is made by evaluating the consensus PDFs for all N_T valid states of the activation vectors, *i.e.*,

$$\hat{\mathbf{e}}_{k_p^R} = \underset{\mathbf{e}_t \in \mathcal{E}}{\text{argmax}} \mathbb{P}(b_p^R | \mathbf{e}_t), \quad (44)$$

which is equivalent to computing the consensus soft-replicas

$$\hat{\mathbf{e}}_{k_p^R} = \frac{\mathbf{r}_p \odot \mathbf{z}_p^R}{\mathbf{r}_p^\top \cdot \mathbf{z}_p^R}, \quad (45)$$

where

$$\mathbf{z}_p^R = \exp_{\odot}(\boldsymbol{\eta}_p^R - \frac{1}{2} \text{diag}(\boldsymbol{\Lambda}_p^R)), \quad (46)$$

and determining the index of the maximum value of the consensus soft-replica, *i.e.*,

$$k_p^R = \underset{t \in \mathcal{T}}{\text{argmax}} (\hat{e}_{k_p^R}^R(t)), \quad (47)$$

where $\hat{e}_{k_p^R}^R(t)$ denote the t -th element of $\hat{\mathbf{e}}_{k_p^R}^R$.

Algorithm 1: Proposed UVD-GaBP GQSM Decoder

Inputs: Received signal \mathbf{y} , effective channels \mathbf{H}^R and \mathbf{H}^I , pilot symbols $s_p^R, s_p^I \forall p$, and noise variance N_0 .

Outputs: Estimated activation vectors $\tilde{\mathbf{e}}_{k_p^R}$ and $\tilde{\mathbf{e}}_{k_p^I}$ $\forall p$.

Initialization: $\forall n$ and $\forall p$,

1: Initialize the soft-replicas $\hat{\mathbf{e}}_{k_p^R:n}, \hat{\mathbf{e}}_{k_p^I:n}$, following the prior PMF of equation (24);

2: Compute $\boldsymbol{\Gamma}_{p:n}^R, \boldsymbol{\Gamma}_{p:n}^I$ via equation (26);

MP iterations until convergence, $\forall n$ and $\forall p$,

3: Perform soft-IC to obtain $\bar{y}_{p:n}^R, \bar{y}_{p:n}^I$ via equation (28);

4: Compute $\nu_{p:n}^R, \nu_{p:n}^I$ via equation (31);

5: Compute $\boldsymbol{\eta}_{p:n}^R, \boldsymbol{\eta}_{p:n}^I$ via equation (34);

6: Compute $\text{diag}(\boldsymbol{\Lambda}_{p:n}^R), \text{diag}(\boldsymbol{\Lambda}_{p:n}^I)$ via equation (39);

7: Compute $\hat{\mathbf{e}}_{k_p^R:n}, \hat{\mathbf{e}}_{k_p^I:n}$ via equation (37);

8: Compute $\boldsymbol{\Gamma}_{p:n}^R, \boldsymbol{\Gamma}_{p:n}^I$ via equation (26);

9: Update $\hat{\mathbf{e}}_{k_p^R:n}, \hat{\mathbf{e}}_{k_p^I:n}, \boldsymbol{\Gamma}_{p:n}^R, \boldsymbol{\Gamma}_{p:n}^I$ with damping via eq. (40);

end for

Belief Consensus: $\forall p$,

10: Obtain $\boldsymbol{\eta}_p^R, \boldsymbol{\eta}_p^I$ via equation (42);

11: Obtain $\text{diag}(\boldsymbol{\Lambda}_p^R), \text{diag}(\boldsymbol{\Lambda}_p^I)$ via equation (43);

12: Obtain $\tilde{\mathbf{e}}_{k_p^R}, \tilde{\mathbf{e}}_{k_p^I}$ via equation (44);

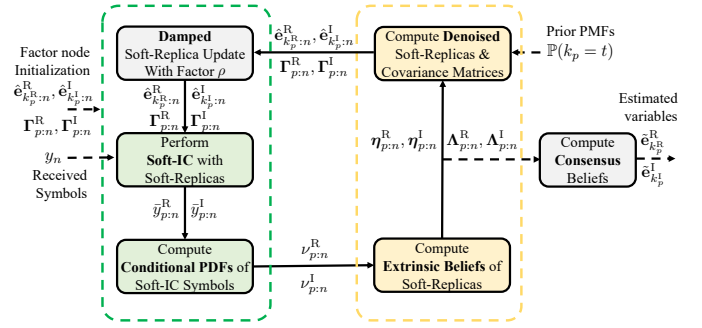


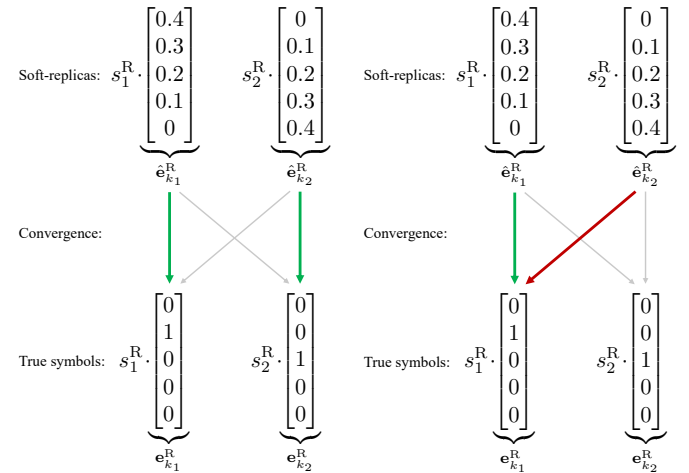
Fig. 3: Schematic diagram of the proposed UVD-GaBP detector. The operations in the factor nodes and the variable node have been illustrated in green and yellow colors, respectively.

The proposed low-complexity decoder hereby dubbed the “UVD-GaBP” for piloted GQSM schemes, described by equation (25)-(47), is summarized by Algorithm 1 and illustrated as a schematic diagram in Figure 3.

V. IMPROVING THE PROPOSED UVD-GaBP DECODER

In this section, the fundamental limitations and the consequent sources of errors of the proposed decoder in Section IV are identified, which mainly arises from the omission of the joint probability information between the unit vectors of the UVD. Subsequently, enhancements to the algorithm are proposed to improve the detection performance against such errors, at the cost of an additional computational complexity yet minimal structural change.

Consider two soft-replicas⁶ $\hat{\mathbf{e}}_{k_p}^R$ and $\hat{\mathbf{e}}_{k_{p'}}^R$ of two unique unit vectors $\mathbf{e}_{k_p}^R$ and $\mathbf{e}_{k_{p'}}^R$ with $p \neq p'$, and the respective transmit symbols s_p^R and $s_{p'}^R$. Correct estimation results in the convergence of the effective symbol $s_p^R \cdot \hat{\mathbf{e}}_{k_p}^R$ to the true value of $s_p^R \cdot \mathbf{e}_{k_p}^R$, and $s_{p'}^R \cdot \hat{\mathbf{e}}_{k_{p'}}^R$ to $s_{p'}^R \cdot \mathbf{e}_{k_{p'}}^R$, as illustrated in Figure 4a.



(a) Correct convergence with uniquely estimated unit vectors. (b) Erroneous convergence with duplicate unit vector estimates.

Fig. 4: Two exemplary cases of unit vector variable convergence, for a GQSM system with $N_T = 5, P = 2$.

⁶Without loss of generality the dependencies on the observation node denoted by the subscript $(\cdot)_n$ are omitted here, and only the real part variables $(\cdot)^R$ are described, as the same analysis applies to the imaginary part variables $(\cdot)^I$.

On the other hand, an erroneous estimation may arise when a soft-replica converges to the wrong unit vector, as illustrated in Figure 4b, leading to a *duplicate* estimate. Due to the combinatoric selection of the indices in a GQSM index vector and of general IM schemes as described in Section II-A, no duplicate indices may exist within a single index vector.

In light of the above, two sources of such erroneous duplicate convergence are identified: *a)* high transmit symbol similarity, and *b)* lack of joint/dependent distribution information between the unit vector variables. In order to mitigate the error from the above identified sources, three modifications to the GQSM transmitter and the UVD-GaBP decoder are proposed in the following.

A. IQ-Orthogonal Constellation Design

Let us assume that multiple transmit symbols have high similarity, *i.e.*, $|s_p^R - s_{p'}^R|^2 \approx 0$. Such behavior is illustrated by observing Fig. 4b and considering $s_p^R \approx s_{p'}^R$, where the initialized effective symbols $s_p^R \cdot \hat{\mathbf{e}}_{k_p}^R$ and $s_{p'}^R \cdot \hat{\mathbf{e}}_{k_{p'}}^R$ are consequently very similar in value. Therefore, the effective symbols appearing in the core MP steps of the UVD-GaBP decoder in equations (28)-(35), may converge to either of the true symbols $s_p^R \cdot \mathbf{e}_{k_p}^R$ or $s_{p'}^R \cdot \mathbf{e}_{k_{p'}}^R$, and potentially produce an erroneous duplicate estimate.

The first proposed approach to mitigate the duplicate convergence error is to modify the transmit symbol constellation, such that a sufficient difference in numerical value are ensured for the symbols in the respective real and imaginary domains.

To that end, consider the IQ-decoupled constellations $\mathcal{S}^R \triangleq \Re\{\mathcal{S}^c\}$ and $\mathcal{S}^I \triangleq \Im\{\mathcal{S}^c\}$, which is equivalent to two PAM constellations respectively on the real and imaginary axes, as illustrated in Figure 5a. For a symmetric M -QAM constellation \mathcal{S}^c , the PAM constellations have a smaller cardinality than M , as multiple symbols in \mathcal{S}^c may convey the same amplitude in the IQ domain, leading to duplicate symbol values.

In order to avoid such duplicate symbols in the IQ domain, we propose a simple rotation scheme to \mathcal{S}^c , which leads to non-duplicate PAM symbols in both IQ domains. Furthermore, an optimal rotation angle θ^* is obtained to maximize the minimum Euclidean distance between the symbols of the PAM constellation. There exist an optimal rotation angle θ^* for each of the quadrants, but we only consider the solution within the first quadrant, *i.e.*, $\theta \in (0, \frac{\pi}{2})$, which are shown in Table I.

The optimization problem is described by

$$\theta^* = \underset{\theta \in (0, \frac{\pi}{2})}{\operatorname{argmax}} D_{\min}(\Re\{e^{j\theta} \cdot \mathcal{S}^c\}) + D_{\min}(\Im\{e^{j\theta} \cdot \mathcal{S}^c\}), \quad (48)$$

where $D_{\min}(\cdot)$ is a function on a set denoting the minimum Euclidean distance of its elements defined as

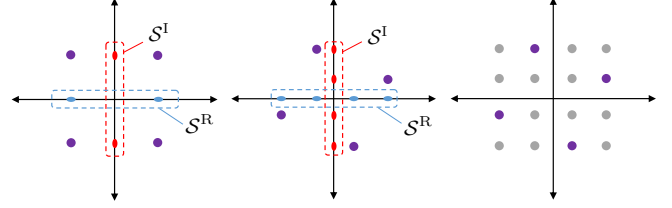
$$D_{\min}(\mathcal{S}) \triangleq \min_{s_m, s_{m'} \in \mathcal{S}} \sqrt{|s_m - s_{m'}|^2}, \quad \forall m \neq m'. \quad (49)$$

It is observed that the optimal rotation illustrated in Figure 5b is effectively equivalent to fitting a QAM constellation from M unique IQ-orthogonal symbols from the a larger scaled QAM constellation to maximize the minimum Euclidean distances between the symbols, as illustrated in Figure 5c.

In light of the above, given that the pilot symbols are selected uniquely, the rotated constellation ensures no duplicate or *similar* symbols in each of the decoupled IQ domain.

TABLE I: Optimal rotation angles θ^* in radians (to the nearest 3 decimal points) for different constellation sizes M .

M	4	16	32	64	128	256
θ^*	0.464	0.245	0.165	0.124	0.082	0.062



(a) Symmetric 4QAM constellation. (b) Optimally rotated 4QAM constellation. (c) Optimal 4QAM constellation within the 16QAM.

Fig. 5: Illustrations of the described complex constellations, where the symbols of the constellation are denoted in purple.

B. Conditional PDF-based Denoiser

In addition to the optimal rotation of the symbol constellation which is a pre-computed at the GQSM transmitter, another approach is proposed to enhance the proposed detector in this section. In order to avoid the duplicate estimation error of the unit vectors the dependent information of the unit vectors can be incorporated in the form of conditional PMFs. Specifically, the prior PMFs $\mathbb{P}_{\mathbf{e}_{k_p}}(\mathbf{e}_{k_p} = \mathbf{e}_t)$ of the Bayes-optimal soft-replica denoiser in equation (36) may be enhanced to first-order⁷s conditional PMFs $\mathbb{P}_{\mathbf{e}_{k_p} | k_{p'}}(\mathbf{e}_{k_p} = \mathbf{e}_t | \mathbf{e}_{k_{p'}} = \mathbf{e}_{t'}) \equiv \mathbb{P}_{\mathbf{e}_{k_p} | k_{p'}}(\mathbf{e}_{k_p} = \mathbf{e}_t | k_{p'} = t')$, for $p \neq p'$ and $t \neq t'$. In other words, the first-order conditional PMFs yield the activation probability of the t -th index of the p -th unit vector, given the activation information of t' -th index of the p' -th unit vector.

However, the evaluation of a conditional PMF requires hard-decided activation indices for a given unit vector, which is not available within the MP iterations fundamentally based on soft-replicas. Therefore within each iteration of the MP algorithm, a greedy hard-determination of the most confident index pair (p, t) is made for each n -th factor node by evaluating equation (33), and finding the index pair yielding the maximal belief mass, *i.e.*, by solving

$$\check{p}_n^R, \check{t}_n^R = \underset{p, t}{\operatorname{argmax}} \mathbb{P}(b_{p:n}^R | \mathbf{e}_t), \quad (50)$$

which is equivalent to obtaining the indices of the maximum values in the belief mass vector $\mathbf{z}_{p:n}^R$ in equation (38).

Under such greedy selection, the conditional PMF-based denoiser with the greedy indices $\check{p}_n^R, \check{t}_n^R$, becomes

$$\begin{aligned} \hat{\mathbf{e}}_{k_p^R : n} &= \frac{\mathbb{E}_{\mathbf{e}_{k_p} | k_{p'}}[\mathbf{e}_{k_p} \cdot \mathbb{P}(b_{p:n}^R | \mathbf{e}_{k_p}) | k_{p'}^R = \check{t}_n^R]}{\mathbb{E}_{\mathbf{e}_{k_p} | k_{p'}}[\mathbb{P}(b_{p:n}^R | \mathbf{e}_{k_p}) | k_{p'}^R = \check{t}_n^R]} \in \mathbb{R}^{N_T \times 1}, \quad (51) \\ &= \frac{\sum_{\mathbf{e}_t \in \mathcal{E}} (\mathbf{e}_t \cdot \mathbb{P}_{\mathbf{e}_{k_p} | k_{p'}}(\mathbf{e}_{k_p} = \mathbf{e}_t | k_{p'} = \check{t}_n) \cdot \mathbb{P}(b_{p:n}^R | \mathbf{e}_{k_p}))}{\sum_{\mathbf{e}_t' \in \mathcal{E}} (\mathbb{P}_{\mathbf{e}_{k_p} | k_{p'}}(\mathbf{e}_{k_p} = \mathbf{e}_t' | k_{p'} = \check{t}_n) \cdot \mathbb{P}(b_{p:n}^R | \mathbf{e}_{k_p}'))}, \end{aligned}$$

to yield the soft-replica vectors incorporating the dependent information of the most confident unit vector variable.

⁷While it is also possible to incorporate higher-order conditional PMFs by incorporating more than one conditional variable, the derivation and application of such higher-order PMFs require a significantly increased computational and space complexity, such that only the first-order conditional PMF is considered in this work for practicality.

The conditional PMFs does not exhibit a closed-form expression unlike equation (23) for the independent PMFs, and therefore must be obtained via numerical evaluation. However, as the conditional PMFs are fixed for a given codebook, *i.e.*, system parameters N_T and P , all values can be pre-computed.

C. Greedy Successive Interference Cancellation (IC)

Furthermore, a similar approach can also be performed after the convergence of the MP iterations to find the index of the strongest value within the converged beliefs in equation (41)

$$\hat{p}^R, \hat{t}^R = \underset{p,t}{\operatorname{argmax}} \mathbb{P}(b_p^R | e_t), \quad (52)$$

which is equivalent to obtaining the indices of the maximum values in the belief masses \mathbf{z}_p^R in equation (46).

In hand of a converged index of the most confident unit vector variable, IC can be performed on the received signals corresponding to the selected indices as

$$\tilde{y}_n^R \triangleq y_n - (\mathbf{h}_n^R)^T (s_{\hat{p}_n^R}^R \cdot \mathbf{e}_{\hat{t}_n^R}), \quad (53)$$

and the corresponding variables are nullified from the respective soft-replica, to be repeated for P successive IC iterations.

Finally, the estimated index vectors can be obtained by concatenating and sorting the inherent activation indices from each greedy selection step without having to evaluate equation (44)-(47), *i.e.*,

$$\tilde{\mathbf{k}}^R = \operatorname{sort}([\hat{t}_{[1]}^R, \dots, \hat{t}_{[P]}^R]), \quad (54)$$

where $\hat{t}_{[\lambda]}^R$ denote the greedily selected activation index at the λ -th iteration of the successive IC loop.

Algorithm 2: Proposed UVD-GaBP GQSM Decoder with Conditional Denoiser and Successive IC

Inputs: Received signal \mathbf{y} , effective channels \mathbf{H}^R and \mathbf{H}^I , pilot symbols $s_p^R, s_p^I \forall p$, and noise variance N_0 .

Outputs: Estimated index vectors $\tilde{\mathbf{k}}^R$ and $\tilde{\mathbf{k}}^I$.

Initialization: $\forall n$ and $\forall p$,

- 1: Initialize the soft-replicas $\hat{\mathbf{e}}_{k_p^R:n}, \hat{\mathbf{e}}_{k_p^I:n}$, following the prior PMF of equation (24);
- 2: Compute $\mathbf{\Gamma}_{p:n}^R, \mathbf{\Gamma}_{p:n}^I$ via equation (26);

Successive IC iterations for $\lambda = 1, \dots, P$,

MP iterations until convergence, $\forall n$ and $\forall p$,

- 3: Perform soft-IC to obtain $\tilde{y}_{p:n}^R, \tilde{y}_{p:n}^I$ via equation (28);
- 4: Compute $\nu_{p:n}^R, \nu_{p:n}^I$ via equation (31);
- 5: Compute $\eta_{p:n}^R, \eta_{p:n}^I$ via equation (34);
- 6: Compute $\operatorname{diag}(\mathbf{\Lambda}_{p:n}^R), \operatorname{diag}(\mathbf{\Lambda}_{p:n}^I)$ via equation (39);
- 7: Evaluate $\tilde{p}_n^R, \tilde{p}_n^I$ and $\tilde{t}_n^R, \tilde{t}_n^I$ via equation (50);
- 8: Compute $\hat{\mathbf{e}}_{k_p^R:n}, \hat{\mathbf{e}}_{k_p^I:n}$ via equation (51);
- 9: Compute $\mathbf{\Gamma}_{p:n}^R, \mathbf{\Gamma}_{p:n}^I$ via equation (25);
- 10: Update $\hat{\mathbf{e}}_{k_p^R:n}, \hat{\mathbf{e}}_{k_p^I:n}, \mathbf{\Gamma}_{p:n}^R, \mathbf{\Gamma}_{p:n}^I$ via damping eq. (40);

end for

Belief Consensus: $\forall p$,

- 11: Obtain η_p^R, η_p^I via equation (42);
- 12: Obtain $\operatorname{diag}(\mathbf{\Lambda}_p^R), \operatorname{diag}(\mathbf{\Lambda}_p^I)$ via equation (43);
- 13: Evaluate \tilde{p}^R, \tilde{p}^I and \tilde{t}^R, \tilde{t}^I via equation (52);
- 14: Store the values of \tilde{p}^R, \tilde{p}^I and \tilde{t}^R, \tilde{t}^I at the λ -th IC iteration.
- 15: Perform IC to obtain $\tilde{y}_n^R, \tilde{y}_n^I$ via equation (53);

end for

Index Vector Evaluation:

- 16: Obtain $\tilde{\mathbf{k}}^R, \tilde{\mathbf{k}}^I$ via equation (54);
-

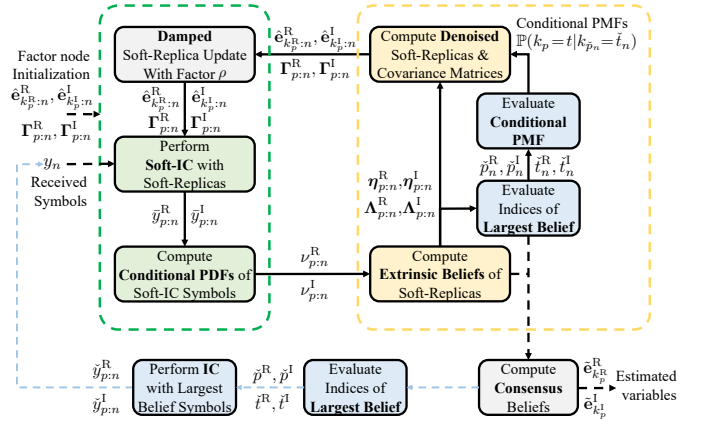


Fig. 6: Schematic diagram of the enhanced UVD-GaBP detector with the conditional denoiser and successive IC operations.

The complete procedure, incorporating the proposed receiver-side enhancements of Sections V-C and V-B, is provided as a pseudocode in Algorithm 2, and as a schematic diagram in Figure 6. Notice that for $P = 1$, the proposed enhancement is not necessary as there is only a single unit vector to evaluate, and the conditional PMF-based denoiser is not applicable as there is no other unit vector to condition the extrinsic beliefs. In addition, the motivation of such enhancements is not necessary for $P = 1$, as the *duplicate convergence* error cannot occur with a single unit vector variable.

VI. PERFORMANCE ANALYSIS

A. BER Performance

To analyze the performance of the proposed UVD-GaBP algorithm and the enhancement modules in Sec. V, we perform simulations for different system sizes characterized by N_T transmit antennas, N_R receive antennas, and P pilot symbols from the M -ary constellation, including truly massive systems with large N_T and N_R . Specifically, three algorithmic cases as summarized in Table II, are selected to capture and highlight the improvements introduced by each of the three proposed enhancement modules, namely: Algorithm 1 as the baseline UVD-GaBP decoder; Algorithm 2 with conditional denoiser but without successive IC; and finally the full Algorithm 2 with both the conditional denoiser and successive IC. Note that the optimized constellations are employed in all cases considered.

To serve as a reference, the results are compared against the matched filter bound (MFB), which corresponds to the performance of a Genie-aided system in which the soft-replicas of the GaBP iterations are initialized with the actual (true) transmitted activation vectors.

Our first set of results, depicted in Figure 7, compares the bit error rate (BER) performances of the proposed UVD-GaBP decoder for all cases in Table II and the corresponding MFB, in MIMO systems of size 32×32 employing various numbers of symbols P .

TABLE II: Selected cases for the numerical evaluation.

	Alg. 1	Alg. 2 (no IC)	Alg. 2
Opt. Constellation (Sec. V-A)	✓	✓	✓
Cond. Denoising (Sec. V-B)		✓	✓
Successive IC (Sec. V-C)			✓

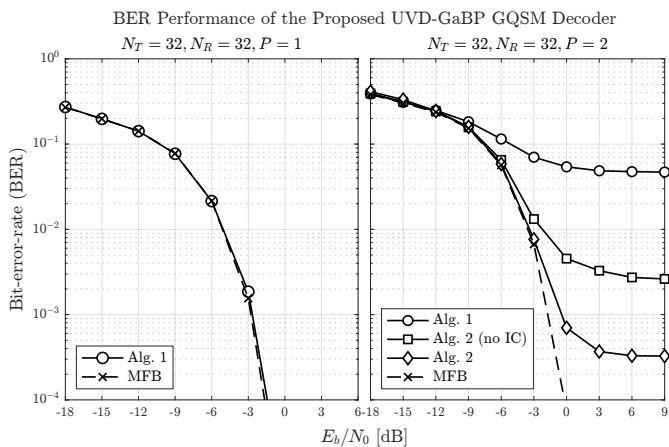
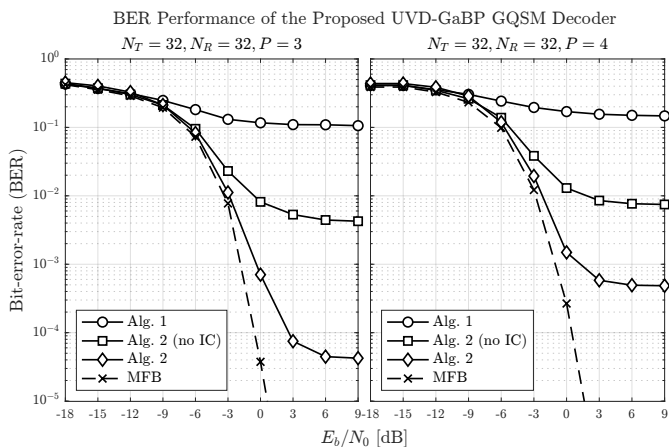
(a) $P = 1$ and $P = 2$.(b) $P = 3$ and $P = 4$.

Fig. 7: The BER performance comparison for the different cases of the proposed UVD-GaBP decoder, with system size parameters $N_T = 32$, $N_R = 32$, $M = 4$.

The BER plots against the energy-per-bit-to-noise-power-spectral-density ratio (E_b/N_0) capture the effects of the duplicate convergence of unit vectors as identified in Section V, highlighting it as a source of errors, which of course does not occur for $P = 1$ but can be substantial for $P > 1$. The results show, however, that this error is successfully mitigated by the improvements described in Sections V-B and V-C.

In addition, the plots also exhibit error-floors for $P > 1$, which still remain while significantly lowered by the proposed enhancement modules. Such error-floor is a convergent phenomenon of MP algorithms in non-ideal high signal-to-noise ratio (SNR) regimes [67], [68], also enlarged when the number of observation nodes is small, i.e., $N_R < N_T$, whose mitigation has been extensively studied via various methods, including adaptive MP updates and post-processing [69], [70]. However, such extra modifications to further reduce the error-floors are not specific to the IM structure and its detection, and therefore have been considered out of scope of this article.

Furthermore, it is found that sufficiently large MIMO system sizes can sustain larger P values with significantly reduced error-floors. In order to demonstrate this, we offer our next set of results, given in Figure 8, which show the performances achieved by Algorithm 2 in truly massive system scales of 64×64 and 96×96 . We remark that simulation results for

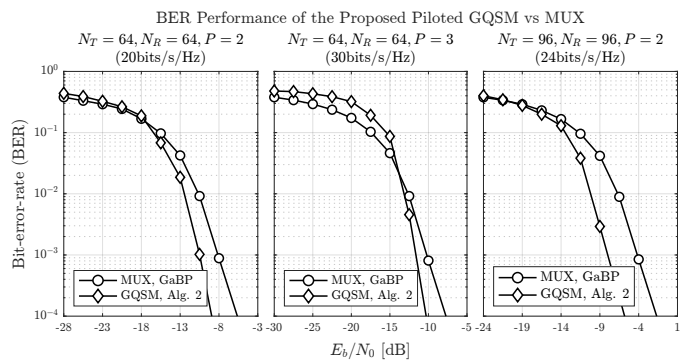


Fig. 8: The BER performance comparison of piloted GQSM-ISAC with the proposed decoder of Algorithm 2 and piloted MUX-ISAC with linear GaBP detection.

GQSM systems of such sizes have never been shown before, precisely due to the prohibitive complexity even with the SotA GQSM detection methods [28], [40].

Notice that Figure 8 also compares the performance of the proposed piloted GQSM scheme against a conventional multiplexed (MUX) MIMO scheme, which in order to enable a fair comparison between the two (proposed and conventional) approaches, the total power and transmission rate (in bits/s/Hz) of both systems have been fixed to identical values, and employ the conventional linear GaBP [65], [69] in the detection of the MUX scheme. It can be seen that, piloted GQSM in massive systems, enabled by the proposed UVD-GaBP detector, outperforms a conventional MIMO-MUX system under equal power and resource constraints, without pilots.

In light of the latter finding, one highly promising application and motivation towards the proposed massive IM framework can be highlighted, which is the efficient incorporation of ISAC via the exploitation of the pilot symbols. Specifically, as the IM framework only embeds information in the index domain and not in the symbols themselves, the sensing functionality can be performed with the known (pilot) symbols via sensing methods available in the literature [15], [58]–[60], [62], [71] without interference from unknown communication symbols, which is known to be a significant challenge in ISAC systems in which decoding errors made on communication symbol estimates may deteriorate sensing performance [72], [73], while channel estimation errors made over pilots may impact on BER performance [74].

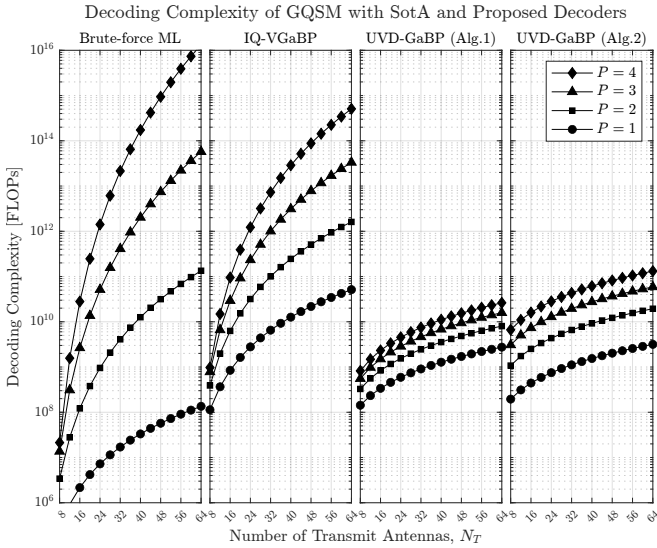
B. Decoding Complexity

In this section, the decoding complexities of the SotA methods, the proposed UVD-GaBP decoder of Sec. IV, and the enhancement modules in Section V are derived, highlighting the significantly reduced complexity, that is completely independent of the prohibitive combinatorial coefficient. Specifically, the computational complexity \mathcal{C} is evaluated in terms of the number of floating point operations (FLOPs), which represents the cost of a single arithmetic operation of a real-valued scalar, and the complexity order $\mathcal{O}(\cdot)$ representing the leading coefficient order of each system parameter variable.

In light of the above, Table III summarizes the decoding complexity of four detection algorithms for piloted GQSM in both the complexity order and relative complexity in FLOPs.

TABLE III: Computational complexity orders of the SotA GQSM decoders the proposed UVD-GaBP decoders.

Algorithm	Complexity Order	Relative Complexity Order
Brute-force ML	$\mathcal{O}[\binom{N_T}{P}^2 N_T N_R]$	$\binom{N_T}{P}^2$
IQ-VGaBP [41]	$\mathcal{O}[\tau \binom{N_T}{P} N_T^2 N_R]$	$\tau \binom{N_T}{P} N_T$
Proposed - Alg. 1	$\mathcal{O}[\tau P^2 N_T^2 N_R^2]$	$\tau P^2 N_T N_R$
Proposed - Alg. 2	$\mathcal{O}[\tau P^3 N_T^2 N_R^2]$	$\tau P^3 N_T N_R$


 Fig. 9: Decoding complexity of the considered algorithms, with varying number of transmit antennas N_T and number of transmit symbols P , fixed $N_R = 64$, and $\tau = 100$.

For the brute-force ML detector, the likelihood metric is evaluated for all codewords of the piloted GQSM codebook \mathcal{X} , and the codeword with the smallest metric is selected, *i.e.*,

$$\hat{\mathbf{x}}_{\text{ML}} = \underset{\mathbf{x} \in \mathcal{X}}{\text{argmin}} \|\mathbf{y} - \mathbf{H}\mathbf{x}\|_2^2, \quad (55)$$

where the required computational complexity in FLOPs is given by equation (56a), which is trivially dependent on the combinatoric full codebook size.

Next, the SotA IQ-decoupled vector-valued GaBP (VGaBP) scheme of [41] is analyzed, which was shown to approach the optimal performance of the ML decoder. Following [41], the decoding complexity of the IQ-decoupled VGaBP is given by equation (56b), with τ number of MP iterations, where a quadratic order complexity reduction is attained by exploiting the half-sized decoupled i.i.d. variables of the GQSM in the IQ domain of equation (8).

Finally, the decoding complexities of the two proposed algorithms are obtained by following each step of the proposed MP rules elaborated in Sections IV and V, which are respectively given by equations (56c) and (56d).

By comparing the complexity order, it can be seen that the intractable combinatorial coefficient of the GQSM is not

inherited by the proposed UVD-GaBP decoders, and instead replaced with a significantly lower polynomial-order complexity order term on the system size parameters P , N_T , and N_R .

Figure 9 compares the full decoding complexity in FLOPs of the four analyzed decoders, for increasing number of transmit antennas N_T and varying values of symbols P . The number of receive antennas N_R and the number of MP iterations τ are fixed respectively at a reasonable value of $N_R = 64$ and $\tau = 100$, as the two parameters only introduce a linear complexity order, as opposed to N_T and P with more prominent effects, as can be seen in the summary of Table III.

For $P = 1$, the combinatorial coefficient $\binom{N_T}{P}$ will reduce to N_T and hence the ML decoder enjoys a significantly low complexity, however, for actual combinatorial IM codebooks even with $P = 2$ or $P = 3$, the complexity of the ML decoder and the IQ-VGaBP is shown to increase to an infeasible order with respect to N_T and P , especially for significantly large scales of the transmitter with $N_T \geq 16$.

On the other hand, the proposed UVD-GaBP while requiring a higher complexity than that of the ML with small N_T and P , a significant superiority can be observed for scenarios with larger system parameters of N_T and P , where the rate of complexity gain with respect to N_T and P is shown to be very low, noting the logarithmic scale of the complexity plot.

While already illustrated by the behavior for the smaller values of $P = 1, 2, 3, 4$, it should also be highlighted that the complexity advantage between the non-combinatorial and combinatorial detectors becomes more significant for increasing values of P , which is not plotted for the sake of visualization. Therefore, when P is parametrized to yield the maximum spectral efficiency, which is $P = N_T/2$ for piloted IM schemes and $P > N_T/2$ for digitally modulated IM schemes such as GQSM [28], [40], the combinatoric-free advantage of the proposed decoders will be more protuberant.

Finally, Figure 10 highlights the superiority of the low-complexity UVD-GaBP enabled piloted GQSM system with respect to the effective gain of the BER performance per decoded bit, in other words, illustrates the comparison of differently parametrized MIMO GQSM with N_T and P , subject to the same decoding complexity cost.

The left subfigure first compares piloted GQSM systems requiring a decoding complexity in the order 2×10^9 FLOPs, with the three selected scenarios: ML decoder with $N_T = 16$, $N_R = 16$, $P = 3$, the enhanced UVD-GaBP decoder (Alg. 2) with $N_T = 24$, $N_R = 24$, and $P = 3$, and the UVD-GaBP decoder (Alg. 1) with $N_T = 32$, $N_R = 32$, and $P = 2$. Similarly, the right subfigure compares piloted GQSM systems requiring a decoding complexity in the order 3×10^{10} FLOPs, with: ML decoder with $N_T = 16$, $N_R = 16$, $P = 4$, the enhanced UVD-GaBP decoder (Alg. 2) with $N_T = 32$, $N_R = 32$, and $P = 4$, and also with $N_T = 48$, $N_R = 48$, and $P = 3$.

$$C_{\text{ML}} \triangleq \binom{N_T}{P}^2 \cdot (8N_R N_T + 4N_R), \quad (56a)$$

$$C_{\text{IQ}} \triangleq \tau (2N_R [\binom{N_T}{P} (15N_T^2 + 15N_T + 4) + 3N_T^2 - 2] + 4N_T^2) + 2N_R (N_T^2 + 2N_T + 1) + \binom{N_T}{P} (6N_T^2 + 9N_T + 2) + 5N_T^2, \quad (56b)$$

$$C_{\text{UVD}} \triangleq \tau \cdot 4N_R P [2P(6N_T^2 + 3N_T - 1) + 6N_T^2 + 8N_T N_R + 4N_T + 4N_R + 1] + P(8N_T N_R + 4N_R + 10N_T + 4), \quad (56c)$$

$$C_{\text{E-UVD}} \triangleq \tau \cdot 4N_R P^2 [2P(6N_T^2 + 3N_T + 2N_T N_R - 1) + 6N_T^2 + 8N_T N_R + 4N_T + 4N_R + 1] + P^2 (12N_T N_R + 4N_R + 10N_T + 4). \quad (56d)$$

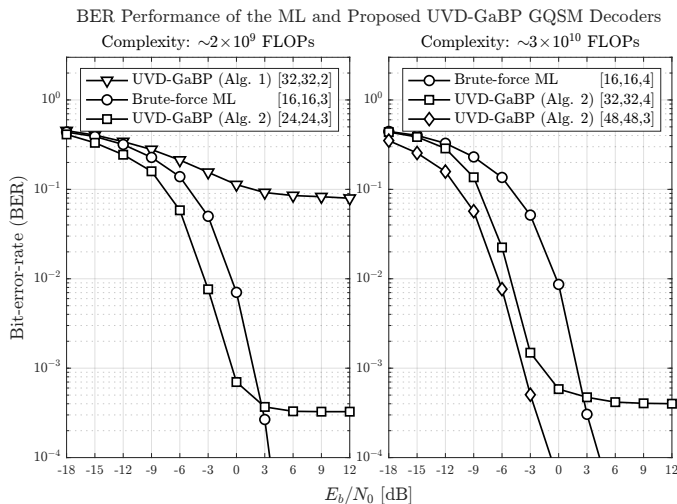


Fig. 10: The BER performance comparison for the ML and UVD-GaBP decoders under varying system size parameters but the approximately same decoding complexities.

In light of the decreased complexity, the supported GQSM system of the UVD-GaBP decoder is able to be significantly scaled especially at larger orders, as compared to the ML decoder. The increased system parameters of N_T and P inherently imply an increased spectral efficiency of the system, improving the BER performance with respect to the E_b/N_0 .

The E_b/N_0 gain is about 3dB in the left figure under a decoding complexity of 2×10^9 FLOPs, and the gain increases for higher complexity scales to 6dB in the right figure under a decoding complexity of 3×10^{10} FLOPs. This E_b/N_0 gain is expected to increase with increasing complexity order, due to the combinatorial growth of the ML decoding complexity, as can be seen in the behavior of Figure 9.

While the error floor behavior is also still present in the proposed decoders as opposed to the ML decoders, the performance up to the error floor is superior, and the error floor is also expected to be mitigated in large systems as shown in the performance analysis of Section VI, or via post-processing techniques as previously discussed.

VII. CONCLUSION

We proposed a new paradigm for feasibly enabling truly massive scales of IM schemes in expectation for the B5G, by proposing a novel detection algorithm which is shown to achieve a decoding complexity that is completely independent of the previously prohibitive combinatorial factor. The proposed scheme is based on a novel UVD formulation of piloted IM signals which is generally applicable to many types of IM schemes, on which the tailored GaBP rules are designed, aided by the novel derivation of the index activation probabilities. In addition, several enhancements to improve the performance of piloted IM with the UVD-GaBP is presented, in the form of transmit symbol constellation optimization and modified MP rules based on conditional PMF-based denoising and successive IC. The effectiveness of the proposed method is verified via simulation results with the GQSM as the exemplary technique, which is shown to

outperform the classical MIMO multiplexing scheme in terms of the BER performance in very large MIMO systems, in addition to showing the reduced complexity of the proposed detector by showing unprecedented GQSM detection results for system sizes up to 96×96 transmit and receive antennas.

REFERENCES

- [1] H. S. Rou, *et al.*, "Enabling energy-efficiency in massive-MIMO: A scalable low-complexity decoder for generalized quadrature spatial modulation," in *IEEE 9th International Workshop on Computational Advances in Multi-Sensor Adaptive Processing*, 2023, pp. 301–305.
- [2] T. S. Rappaport *et al.*, "Wireless communications and applications above 100 GHz: Opportunities and challenges for 6G and beyond," *IEEE Access*, vol. 7, pp. 78 729–78 757, 2019.
- [3] N.-S. Vo, T. Q. Duong, and Z. Sheng, "The key trends in B5G technologies, services and applications," *Mobile Networks and Applications*, vol. 27, no. 4, pp. 1716–1718, 2022.
- [4] M. A. Uusitalo *et al.*, "6G vision, value, use cases and technologies from european 6G flagship project Hexa-X," *IEEE Access*, vol. 9, pp. 160 004–160 020, 2021.
- [5] C.-X. Wang *et al.*, "On the road to 6G: Visions, requirements, key technologies and testbeds," *IEEE Commun. Surveys & Tuts.*, 2023.
- [6] S. Tripathi, N. V. Sabu, A. K. Gupta, and H. S. Dhillon, "Millimeter-wave and terahertz spectrum for 6G wireless," in *6G Mobile Wireless Networks*. Springer, 2021, pp. 83–121.
- [7] H.-J. Song and N. Lee, "Terahertz communications: Challenges in the next decade," *IEEE Trans. THz Sci. Technol.*, vol. 12, no. 2, 2022.
- [8] Y. Huo *et al.*, "Technology trends for massive MIMO towards 6G," *Sensors*, vol. 23, no. 13, p. 6062, 2023.
- [9] H. He *et al.*, "Cell-free massive MIMO for 6G wireless communication networks," *Journ. Commun. Inf. Net.*, vol. 6, no. 4, pp. 321–335, 2021.
- [10] H. Zhang, B. Di, L. Song, and Z. Han, *Reconfigurable intelligent surface-empowered 6G*. Springer, 2021.
- [11] C. Pan *et al.*, *et al.*, "Reconfigurable intelligent surfaces for 6G systems: Principles, applications, and research directions," *IEEE Communications Magazine*, vol. 59, no. 6, pp. 14–20, 2021.
- [12] F. Liu *et al.*, "Integrated sensing and communications: Toward dual-functional wireless networks for 6G and beyond," *IEEE Journal on Selected Areas in Communications*, vol. 40, no. 6, pp. 1728–1767, 2022.
- [13] J. Wang *et al.*, "Integrated sensing and communication: Enabling techniques, applications, tools and data sets, standardization, and future directions," *IEEE Internet of Things Journal*, vol. 9, no. 23, 2022.
- [14] Z. Wei *et al.*, "Integrated sensing and communication signals toward 5G-A and 6G: A survey," *IEEE Internet of Things Journal*, vol. 10, no. 13, pp. 11 068–11 092, 2023.
- [15] H. S. Rou *et al.*, "From Orthogonal Time-Frequency Space to Affine Frequency-Division Multiplexing: A comparative study of next-generation waveforms for integrated sensing and communications in doubly dispersive channels," in *IEEE Signal Processing Magazine [Special Issue on Signal Processing for the Integrated Sensing and Communications Revolution]*, vol. 41, no. 5, pp. 71–86, Sept. 2024.
- [16] M. Mandloi, A. Datta, and V. Bhatia, "Index modulation techniques for 5G and beyond wireless systems," *5G and Beyond Wireless Systems: PHY Layer Perspective*, pp. 63–83, 2021.
- [17] T. Mao, Q. Wang, Z. Wang, and S. Chen, "Novel index modulation techniques: A survey," *IEEE Communications Surveys and Tutorials*, vol. 21, no. 1, pp. 315–348, 2019.
- [18] N. Ishikawa *et al.*, "50 years of permutation, spatial and index modulation: From classic RF to visible light communications and data storage," *IEEE Commun. Surv. Tuts.*, vol. 20, no. 3, pp. 1905–1938, 2018.
- [19] X. Cheng *et al.*, "Index modulation for 5G: Striving to do more with less," *IEEE Wireless Communications*, vol. 25, no. 2, pp. 126–132, 2018.
- [20] S. Sugiura, T. Ishihara, and M. Nakao, "State-of-the-art design of index modulation in the space, time, and frequency domains: Benefits and fundamental limitations," *IEEE Access*, vol. 5, pp. 21 774–21 790, 2017.
- [21] M. Wen *et al.*, "On the achievable rate of OFDM with index modulation," *IEEE Trans. Sig. Proc.*, vol. 64, no. 8, pp. 1919–1932, 2015.

- [22] M. Wen *et al.*, "Multiple-mode orthogonal frequency division multiplexing with index modulation," *IEEE Trans. Commun.*, vol. 64, no. 9, pp. 3892–3906, 2017.
- [23] J. Li *et al.*, "Composite multiple-mode orthogonal frequency division multiplexing with index modulation," *IEEE Trans. Wireless Commun.*, vol. 22, no. 6, pp. 3748–3761, 2022.
- [24] Q. Li *et al.*, "Subcarrier index modulation for future wireless networks: Principles, applications, and challenges," *IEEE Wireless Communications*, vol. 27, no. 3, pp. 118–125, 2020.
- [25] R. Y. Mesleh *et al.*, "Spatial modulation," *IEEE Trans. Veh. Technol.*, vol. 57, no. 4, pp. 2228–2241, Jul. 2008.
- [26] A. Younis *et al.*, "Generalised spatial modulation," in *Proc. 44th Asilomar Conf. Signals, Syst. Comput.*, 2010, pp. 1498–1502.
- [27] M. Wen *et al.*, "A survey on spatial modulation in emerging wireless systems: Research progresses and applications," *IEEE Journ. Sel. Areas Commun.*, vol. 37, no. 9, pp. 1949–1972, 2019.
- [28] H. S. Rou *et al.*, "Scalable quadrature spatial modulation," *IEEE Trans. on Wireless Commun.*, vol. 21, no. 11, pp. 9293–9311, 2022.
- [29] A. Raafat, A. Agustín, and J. Vidal, "Downlink multi-user massive MIMO transmission using receive spatial modulation," *IEEE Transactions on Wireless Communications*, vol. 19, no. 10, pp. 6871–6883, 2020.
- [30] J. Li *et al.*, "Index modulation multiple access for 6G communications: Principles, applications, and challenges," *IEEE Network*, vol. 37, no. 1, pp. 52–60, 2023.
- [31] Z. Sui *et al.*, "RIS-assisted cell-free massive MIMO relying on reflection pattern modulation," *IEEE Trans. Commun.*, 2024.
- [32] D. Ma *et al.*, "FRaC: FMCW-based joint radar-communications system via index modulation," *IEEE J. Sel. Topics Signal Process.*, vol. 15, no. 6, pp. 1348–1364, 2021.
- [33] S. Gopi, S. Kalyani, and L. Hanzo, "Intelligent reflecting surface assisted beam index-modulation for millimeter wave communication," *IEEE Trans. on Wireless Commun.*, vol. 20, no. 2, pp. 983–996, 2021.
- [34] H. S. Rou *et al.*, "AFDM Chirp-Permutation-Index Modulation with Quantum-Accelerated Codebook Design", *2024 58th Asilomar Conference on Signals, Systems, and Computers*, 2024.
- [35] B. Shamasundar *et al.*, "On the capacity of index modulation," *IEEE Trans. on Wireless Commun.*, vol. 21, no. 11, pp. 9114–9126, 2022.
- [36] D. Ma *et al.*, "Spatial modulation for joint radar-communications systems: Design, analysis, and hardware prototype," *IEEE Transactions on Vehicular Technology*, vol. 70, no. 3, pp. 2283–2298, 2021.
- [37] A. El-Mai *et al.*, "Efficient joint radar and communication exploiting sparsity and spatial modulation," in *IEEE CAMSAP Workshops*, 2023.
- [38] Z. Hu, F. Chen, Y. Liu, S. Liu, H. Yu, and F. Ji, "Low-complexity detection for multiple-mode ofdm with index modulation," *Physical Communication*, vol. 34, pp. 38–47, 2019.
- [39] L. Wang and Z. Chen, "Enhanced diversity-achieving quadrature spatial modulation with fast decodability," *IEEE Trans. Veh. Technol.*, vol. 69, no. 6, pp. 6165–6177, 2020.
- [40] J. An *et al.*, "The achievable rate analysis of generalized quadrature spatial modulation and a pair of low-complexity detectors," *IEEE Trans. on Veh. Technol.*, vol. 71, no. 5, pp. 5203–5215, 2022.
- [41] H. S. Rou *et al.*, "An efficient vector-valued belief propagation decoder for quadrature spatial modulation," in *2022 56th Asilomar Conference on Signals, Systems, and Computers*, 2022, pp. 27–31.
- [42] S. Katla *et al.*, "Deep learning assisted detection for index modulation aided mmWave systems," *IEEE Access*, vol. 8, 2020.
- [43] J. Kim, H. Ro, and H. Park, "Deep learning-based detector for dual mode OFDM with index modulation," *IEEE Wireless Communications Letters*, vol. 10, no. 7, pp. 1562–1566, 2021.
- [44] K. Yuki Yoshi *et al.*, "Grover adaptive search for maximum-likelihood detection of generalized spatial modulation," *IEEE VTC-Fall*, 2024.
- [45] R. Mesleh *et al.*, "Quadrature spatial modulation," *IEEE Trans. Veh. Technol.*, vol. 64, no. 6, pp. 2738–2742, Jun. 2015.
- [46] L. Xiao *et al.*, "Compressive sensing assisted generalized quadrature spatial modulation for massive MIMO systems," *IEEE Transactions on Communications*, vol. 67, no. 7, pp. 4795–4810, 2019.
- [47] N. Ishikawa, "Quantum speedup for index modulation," *IEEE Access*, vol. 9, pp. 111 114–111 124, 2021.
- [48] S. P. Boyd and L. Vandenberghe, *Convex optimization*. Cambridge university press, 2004.
- [49] L. Xiao *et al.*, "Efficient compressive sensing detectors for generalized spatial modulation systems," *IEEE Trans. on Veh. Technol.*, vol. 66, no. 2, pp. 1284–1298, 2017.
- [50] L. Xiao *et al.*, "Compressive sensing assisted generalized quadrature spatial modulation for massive MIMO systems," *IEEE Transactions on Communications*, vol. 67, no. 7, pp. 4795–4810, 2019.
- [51] T. Van Hong Nguyen, S. Sugiura, and K. Lee, "Low-complexity sphere search-based adaptive spatial modulation," *IEEE Transactions on Vehicular Technology*, vol. 67, no. 8, pp. 7836–7840, 2018.
- [52] C. Li *et al.*, "Quadrature spatial modulation with the fourth order transmit diversity and low-complexity sphere decoding for large-scale MIMO systems," *IEEE Trans. Veh. Tech.*, vol. 71, no. 8, 2022.
- [53] P. Yang *et al.*, "Transmit precoded spatial modulation: Maximizing the minimum euclidean distance versus minimizing the bit error ratio," *IEEE Trans. on Wireless Commun.*, vol. 15, no. 3, pp. 2054–2068, 2016.
- [54] P. Cheng *et al.*, "A unified precoding scheme for generalized spatial modulation," *IEEE Trans. on Commun.*, vol. 66, no. 6, 2018.
- [55] P. Linz, *Theoretical Numerical Analysis: An Introduction to Advanced Techniques*. Dover Publications Inc., 2019.
- [56] J. Riordan, *Introduction to Combinatorial Analysis*. Dover Publications Inc., 2002.
- [57] P. Sablonnière, "Discrete bernstein bases and hahn polynomials," *Journ. of Comp. and Appl. Math.*, vol. 49, no. 1-3, pp. 233–241, 1993.
- [58] L. Gaudio *et al.*, "On the effectiveness of OTFS for joint radar parameter estimation and communication," *IEEE Transactions on Wireless Communications*, vol. 19, no. 9, pp. 5951–5965, 2020.
- [59] K. R. R. Ranasinghe, H. S. Rou and G. T. F. de Abreu, "Fast and Efficient Sequential Radar Parameter Estimation in MIMO-OTFS Systems," *IEEE ICASSP 2024*, Seoul, Korea, Republic of, 2024, pp. 8661–8665
- [60] K. R. R. Ranasinghe *et al.*, "Joint Channel, Data and Radar Parameter Estimation for AFDM Systems in Doubly-Dispersive Channels," *arXiv preprint arXiv:2405.16945*, 2024.
- [61] H. S. Rou *et al.*, "Asymmetric bilinear inference for joint communications and environment sensing," in *2022 56th Asilomar Conference on Signals, Systems, and Computers*, 2022, pp. 1111–1115.
- [62] H. S. Rou, G. T. F. de Abreu, D. González G., and O. Gonsa, "Integrated sensing and communications for 3D object imaging via bilinear inference," *IEEE Trans. on Wireless Commun.*, 2024.
- [63] J. T. Parker, P. Schniter, and V. Cevher, "Bilinear generalized approximate message passing—part I: Derivation," *IEEE Trans. Signal Process.*, vol. 62, no. 22, pp. 5839–5853, 2014.
- [64] K. Ito *et al.*, "Bilinear gaussian belief propagation for massive MIMO detection with non-orthogonal pilots," *IEEE Trans. on Commun.*, 2023.
- [65] P. Som *et al.*, "Improved large-MIMO detection based on damped belief propagation," in *IEEE Inf. Theory Workshop on Inf. Theory*, 2010.
- [66] Q. Su and Y.-C. Wu, "On convergence conditions of gaussian belief propagation," *IEEE Trans. on Sig. Proc.*, vol. 63, no. 5, 2015.
- [67] C. Schlegel and S. Zhang, "On the dynamics of the error floor behavior in (regular) LDPC codes," *IEEE Transactions on Information Theory*, vol. 56, no. 7, pp. 3248–3264, 2010.
- [68] C. Knoll, "Understanding the Behavior of Belief Propagation: Convergence Properties, Approximation Quality, and Solution Space Analysis", *arXiv preprint arXiv:2209.05464*, 2019.
- [69] T. Takahashi, S. Ibi and S. Sampei, "Design of Adaptively Scaled Belief in Multi-Dimensional Signal Detection for Higher-Order Modulation," *IEEE Trans. Commun.*, vol. 67, no. 3, pp. 1986–2001, 2019.
- [70] Z. Zhang *et al.*, "Lowering LDPC Error Floors by Postprocessing," *IEEE GLOBECOM*, New Orleans, LA, USA, 2008, pp. 1-6.
- [71] M. Hua *et al.*, "Integrated sensing and communication: Joint pilot and transmission design," *IEEE Trans. Wireless Commun.*, 2024.
- [72] D. Mi *et al.*, "Massive MIMO performance with imperfect channel reciprocity and channel estimation error," *IEEE Transactions on Communications*, vol. 65, no. 9, pp. 3734–3749, 2017.
- [73] P. Xu, J. Wang, and J. Wang, "Effect of pilot contamination on channel estimation in massive MIMO systems," in *International Conference on Wireless Communications and Signal Processing*, 2013.
- [74] S. Sugiura and L. Hanzo, "Effects of channel estimation on spatial modulation," *IEEE Sig. Proc. Lett.*, vol. 19, no. 12, 2012.